ORIGINAL RESEARCH ARTICLE

Investigation of Aluminum Electrospark Alloyed Coatings on Steels

OKSANA HAPONOVA, VIACHESLAV TARELNYK, NATALIIA TARELNYK, and GENNADII LAPONOG

The paper presents a study of the structure-phase state of aluminised coatings obtained by the electrospark alloying (ESA) method. The influence of the discharge energy and the productivity of the treatment process on the thickness of the hardened layer, its microhardness, continuity and surface roughness of C20 and C40 steels has been studied. It is shown that the structure of ESA coatings consists of a white layer, a diffusion zone and a substrate metal. Increasing the discharge energy during ESA leads to a change in the chemical and phase composition of the layer. With a 2-fold decrease in ESA productivity, the thickness of the ''white'' layer increases to 75 to 110 μm, its microhardness to 7450 MPa; the continuity of the coating tends to 100 pct. With a 4-fold decrease in ESA productivity, the thickness of the 'white' layer also increases, but not intensively, to 60 μm at $W_p = 4.6$ J and then does not change; at the same time, the surface roughness Ra increases to 8.1 to 9.0 μm and the continuity is 95 pct. A 4-fold decrease in process productivity contributes to the deterioration of coating quality parameters and an increase in roughness. The study of the influence of the energy parameters of ESA, as well as the alloying time ('productivity') of the process, is important for the improvement of hardening technology. The paper proposes a mathematical model for predicting the coating parameters taking into account the processing time of a given plane to be alloyed, *i.e.*, the labour intensity of the ESA process (the value of the inverse productivity). The equations of the mathematical model and methods for determining the constants of the equations for predicting the parameters of the alloyed layer have been obtained. An algorithm has been developed and the adequacy of the mathematical model has been verified, which allows the prediction of the main technological parameters of ESA in order to obtain a coating with the specified quality indicators.

https://doi.org/10.1007/s11661-025-07908-z

I. INTRODUCTION

In recent years, environmentally friendly and resource-efficient technological processes have been developed and implemented to increase the service life and reliability of components and tools and to ensure their performance in harsh environments.[1–3] In many cases, modifying the physical and chemical properties of the surface layer of structural materials and products is a sufficient and cost-effective way to improve their performance, as the weakest element in the material-working environment system is the material surface. This highlights the importance of developing methods and technologies for applying protective coatings to the surface of materials. The need for coatings on parts operating at elevated temperatures can be justified by the impossibility of the required increase in the physical and chemical properties of components and parts, even when using new materials with an improved set of chemical, physical, mechanical and other properties.

Promising methods of surface strengthening and modification are methods based on treatment with concentrated flows of energy and matter (CFE).[4,5] Electrospark alloying (ESA) is one of the modern methods of processing metal surfaces of CFE, which allows obtaining surface structures with unique physical, mechanical and tribological properties.[6] The advantage of ESA is the environmental safety of the process, high adhesion strength of the alloyed layer and the substrate

OKSANA HAPONOVA is with the Department of Experimental Mechanics, Institute of Fundamental Technological Research Polish Academy of Sciences, Pawińskiego 5B, 02-106 Warsaw, Poland and also with the Applied Material Science and Technology of Constructional Materials Department, Sumy State University, Kharkivska 116, Sumy 40007, Ukraine. Contact e-mail: gaponova@pmtkm.sumdu.edu.ua VIACHESLAV TARELNYK and NATALIIA TARELNYK are with the Technical Service Department, Sumy National Agrarian University, H. Kondratiieva 160, Sumy 40021, Ukraine. GENNADII LAPONOG is with the Applied Material Science and Technology of Constructional Materials Department, Sumy State University.
Manuscript submitted January 8, 2025; accepted June 28, 2025.
Article published online July 16, 2025

material, the possibility of applying any conductive materials to the surface, low-energy consumption of the process, and ease of technological operations. Electrospark alloying, having wide possibilities of formation in the surfaces of a certain structure, phase and chemical composition, allows to improve their operational properties.

II. LITERATURE REVIEW

Literature and patent sources contain an increasing number of works related to the study of processes occurring in the surfaces of parts,[7,8] the improvement of known ones[9,10] and the development of new technologies[11,12] that allow to control the quality parameters of the surface layers of parts in the required direction. New composite materials consisting of a cheaper and easier to manufacture substrate material and having a surface layer formed using advanced, low-energy and environmentally friendly technology are not inferior and in some respects (durability, cost, consumption of cutting tools and equipment, presence of alloying elements, *etc*.) they are even better than the existing ones.

One of the most popular methods of surface modification is alitisation, which is used to provide iron–carbon alloys with increased resistance to scale, atmospheric corrosion and a range of other properties.

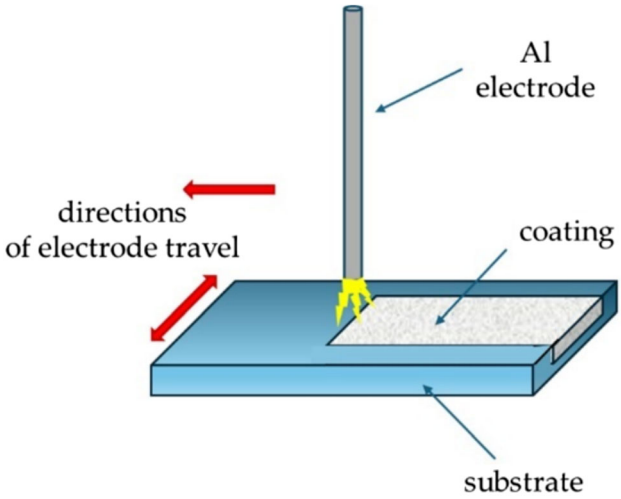

Fig. 1—ESA alitisation scheme.

In addition, complex coatings after alitisation[13,14] are characterised by high melting point, low density, high modulus of elasticity, heat resistance, oxidation and ignition resistance. Recently they have also been used to make protective and wear-resistant coatings.

The classical alitisation technology is diffusion saturation. The application of this technology has been used to study the structure and phase composition of the coating,[15] as well as its effect on the structure and properties of the products after alitisation of structural steels in molten aluminium. Despite the positive results, classical aliteration technology has a number of disadvantages inherent to diffusion methods.[16]

Technologies that use concentrated energy flows (CEF) for material processing occupy a special place among hardening technologies. The use of CEF creates non-equilibrium heating and cooling conditions in the surface. This leads to the formation of structures that are fundamentally different from those produced by traditional processing methods. These are plasma technologies[17,18] and laser processing.[19,20] This group includes one of the most promising modern technologies, the application of which makes it possible to control the quality parameters of the surfaces of parts—electrospark alloying (ESA). ESA technology creates structures in the surface layers of components with unique physical, mechanical and tribological properties at the nano level.[21]

The essence of the ESA process is the erosion of the anode material by spark discharge in a gaseous medium and the transfer of the erosion products to the cathode. On the surface of the cathode, a layer with a modified structure and composition is formed due to the transfer and diffusion of the material as well as to the effect of the thermal and mechanical impulses generated during the electrospark alloying process. As a result of the action of a pulse, craters are formed on the anode and cathode in the gaseous medium. However, under the influence of a spark discharge in a gaseous medium, differences in crater formation are observed due to a more intensive transfer of eroded material to the opposite electrode, especially the cathode. The craters formed on the cathode by the interaction of the transferred anode, cathode material and the inter-electrode medium are filled to varying degrees by the formed material. This material is different from the substrate material. It is not amenable to etching with the reagent intended for the substrate material. The reason for the different phenomena at the anode and the cathode is that the spark discharge energy released at the anode is

Table I. ESA Modes Using the "Traditional" Method ("Elitron-52A")

Mode Number	Discharge Energy, W_p (J)	Voltage (V)	Capacitance, C (μF)	Productivity (cm^2/min)
1	0.52	75	300	1.0 to 1.3
2	1.30	95	480	1.3 to 1.5
3	2.60	75	1560	1.5 to 2.0
4	4.60	100	1560	2.0 to 2.5
5	6.80	210	2040	2.5 to 3.0

Table II. ESA Modes According to the Second Method

Discharge Energy (W_p), J	0.52	1.3	2.6	4.6	6.8
Productivity (cm^2/min)					
1st Option	0.5 to 0.6	0.6 to 0.7	0.7 to 1.0	1.0 to 1.2	1.2 to 1.5
2nd Option	0.2 to 0.3	0.3 to 0.4	0.4 to 0.5	0.5 to 0.6	0.6 to 0.7

an order of magnitude higher than that released at the cathode. This results in the formation of a larger crater on the anode. The influence of thermomechanical factors is also less.

The method of electrospark alloying allows to treat near-surface layers of widely used construction materials based on iron, titanium, aluminium by applying metals, hard alloys, superhard materials to the surface; to change the chemical and phase composition of the surface in a given direction by alloying with metals, intermetallics, compounds, graphite in order to increase corrosion resistance, wear resistance, change electrical resistance, emission-adsorption, thermophysical and other properties; to vary in a given direction microcrystalline, macrocrystalline, nanostructure of near-surface layers of materials; to restore the geometrical dimensions of machine parts and tools with the simultaneous hardening of the surface.

The main advantages of ESA technology compared to traditional surface treatment methods are: environmental and human safety, application in local areas where there is no need to protect neighbouring surfaces from the negative effects of the process, high adhesion of the applied metal, absence of distortion and deformation, and the ability to be integrated into any technological process.[22,23]

Electrospark alloying (ESA) as a method of applying functional coatings compares favourably with other methods such as laser treatment, thermal spraying and traditional diffusion saturation. Studies[24,25] show that ESA can effectively increase the wear resistance, hardness and corrosion resistance of surfaces without the need for sophisticated vacuum equipment or high temperature furnaces. The process is technologically simple, economically feasible and environmentally friendly. It does not produce significant waste or gas emissions.[12]

At the same time, due to the pulsed nature of the discharge, the thermal impact zone in ESA is significantly smaller than in laser or arc processing, reducing the risk of deformation of the substrate material.[26] Unlike laser deposition, ESA allows small areas to be processed without changing the geometry of the part. When machining bearings, tools or hydraulic cylinder components, ESA coatings show a lower coefficient of friction and longer service life compared to analogues produced by traditional surface treatment methods.[27] In addition, numerous studies have confirmed the high corrosion resistance of coatings produced by the ESA.[28]

The disadvantages of ESA are an increase in surface roughness and unevenness, pores in the surface layer, residual tensile stresses and a reduction in fatigue strength.[29,30] It should be noted that as a result of the subsequent surface plastic deformation treatment, these disadvantages are eliminated and the fatigue strength becomes higher than before the ESA treatment.[31,32]

The disadvantages of the ESA method are sometimes attributed to the limited formation of surface layers in thickness. However, there are technologies that can be used to obtain wear-resistant coatings of high quality (100 pct continuity and thickness up to 1.0 mm or even more).[33]

As shown in References 34, 35, aluminium electrospark coatings reliably protect steel from corrosion damage. In addition, complex coatings after alitisation[36] are characterised by a high melting point, low density, high modulus of elasticity, heat resistance, oxidation and ignition resistance. Recently, they have also been used to create protective and wear-resistant coatings. Diffusion methods of alitisation are known.[35,37,38] In this technique, the surface is saturated with aluminium in an aluminium melt.

The authors have shown that as a result of alitisation by dipping in molten aluminium, a layer of metastable $FeAl_m$ and multiple twinned $Al_{13}Fe_4$ phases is formed at the steel–coating interface.[39] However, it is very difficult to control the thickness of the layer and hence the quality of the coating using this technology, because aluminium is a low-melting metal that crystallises quickly on the surface, making it difficult to remove its excess. The authors of Reference 37 suggested that after dipping in a liquid aluminium bath, the subsequent heat treatment should be carried out. However, such a technology requires an additional technological step, which may have limitations in industrial applications due to certain constraints: increased energy consumption, labour intensity, increased technological processing time, inability to process only the required surfaces of parts, *etc*.

Other alitisation techniques are also known. For example, the alitisation method involves applying a layer of aluminium to a steel surface (usually by spraying), plastering and annealing. In this case, particular attention is paid to the roughness of the surface to be aluminised, with oxide films, oil and dust being unacceptable. Despite the positive results, the technology described, as well as the traditional melt aluminisation technology, has a number of disadvantages inherent in the diffusion process. These are bowing and deformation; cumbersome and expensive technological equipment; duration of the process, use of

energy-intensive equipment, *etc*. In addition, certain operations are unsafe for the environment.[40] Therefore, other methods are being developed as an alternative. The ESA method does not have the considered limitations and disadvantages and can be proposed for obtaining aluminised coatings on steels.

The analysis of the relevant literature and patent sources, as well as a number of studies by the authors of this paper,[41,42] has shown that the discharge energy (W_p) has been investigated in the study of the parameters of operation of ESA devices in a wide range and the productivity in accordance with the recommendations.[41] It should be noted that the productivity parameters used are more suitable when hard wear-resistant metals (vanadium, titanium, tungsten, *etc*.) are used as the tool electrode material, so it is scientifically and practically expedient to conduct studies on the effect of ESA productivity in a wider range of alloying times on the quality parameters of the formed surface layer when using an aluminium tool electrode.

It is therefore relevant to:

- Investigation the effect of the productivity of the process of electrospark alloying of steel surfaces with an aluminium tool electrode on the structure formation and quality parameters of the surface layer of steels after alloying;
- Development of a mathematical model that allows the prediction of the main technological parameters of ESA in order to obtain a coating with specified quality parameters.

III. RESEARCH METHODOLOGY

Samples of C20 and C40 steels (carbon contents of 0.2 and 0.4 pct, respectively) with dimensions of 15 mm × 15 mm × 8 mm were used as substrate.

Electrospark alloying was carried out using an Elitron-52A ESA unit, which provides a discharge energy W_p in the range 0.05 to 6.80 J in an air medium. Aluminium was deposited with an uncoated electrode tool using an aluminium wire with a diameter of 3.0 mm.

Two methods of alitisation by the ESA method were studied. The treatment scheme is shown in Figure 1.

The first, the "traditional" technique, consisted in treating the surface of the samples with an aluminium electrode according to the generally accepted modes given in Table I. The alloying modes (voltage, capacitance) correspond to a certain discharge energy specified in the device data sheet.

The productivity in this investigation was defined as the ratio of the surface area treated per unit time (cm^2/min). This means that the value was obtained by dividing the known treated area (1 cm^2) by the actual treatment time. The time was measured using a stopwatch for each alloying mode. Productivity ranges were established for each ESA regime. These values are shown in Tables I and II. This approach ensures consistency in the interpretation of the effect of productivity as an independent treatment variable.

The second technique of alitisation by the ESA method consisted in treating the surface of the samples with an aluminium electrode according to the reduced values of productivity.

Deposition productivity is the area treated per unit time (cm^2/min). Increasing the treatment time (min) decreases the productivity of the ESA. When using ESA in practice, it is difficult to determine the optimum specific alloying time. This is due to the non-linear change in the total weight gain of the sample (mass transfer) with increasing treatment time. The increase in weight gain occurs up to a certain alloying time, after which the deposited coating may be destroyed and the increase stops. Therefore, the optimum alloying time (ESA productivity) is an important technological parameter of the treatment.

The second technique treatment aimed to isolate the effect of productivity as an independent variable while keeping the discharge energy constant. This was done by applying reduced productivity values for each discharge energy.

Table II shows the treatment options for the second technique:

- the first, when the productivity was reduced by ~ 2 times;
- the second, when the productivity was reduced by ~ 4 times.

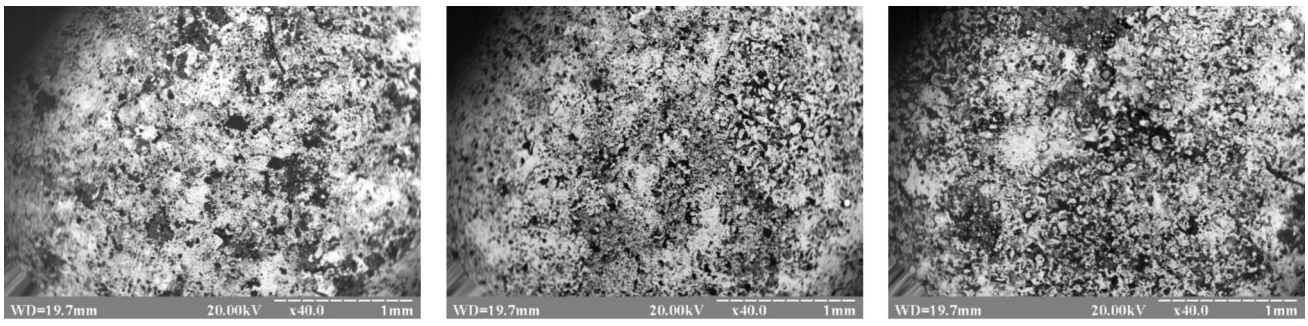

Fig. 2—Aluminised coating morphology on C20 steel after ESA at discharge energies: (*a*) 0.52 J, (*b*) 1.30 J, and (*c*) 2.6 J.

Similar studies will allow the influence of not only discharge energy but also another important parameter of the ESA process—productivity—on the structural and phase state of the coatings to be assessed.

The current is measured by an ammeter on the panel of the ESA unit. The discharge energy (W_p) is calculated using the following formula[43]

$$W_p = k\frac{C \times U^2}{2},$$

where k is a coefficient that takes into account circuit losses (k = 0.6 to 0.7); C is the storage capacitor capacitance, F; U is the no-load voltage, V.

To assess the surface roughness of each sample, five independent scans were taken using the Profilograph-Profilometer mod. 201 of the "Kalibr" company by taking and processing profilograms. The mean and standard deviation were calculated.

Metallographic analysis of the coatings was performed using a Neophot 21 optical microscope and an SEO-SEM Inspect S50-B scanning microscope equipped with an X-MaxN20 detector (Oxford Instruments plc). The SEM was also used for local micro-X-ray spectral analysis of the coatings. Coating continuity was analysed on optical microscopy specimens using stereometric metallography methods. Microhardness was determined using a PMT-3 device, the load was 20 g. A minimum of five indentations were made in representative areas of

Table III. Parameters of the Alitised ESA Coatings According to the Regimes Shown in Table I

	Thickness (μm)		Microhardness, H_μ (MPa)		Roughness (μm)			
W_p (J)	"White" Layer	Diffusion Zone	"White" Layer	Diffusion Zone	Ra	R_Z	R_{max}	Continuity of the "white" Layer (Pct)
Steel C20								
0.52	10 to 12	20 to 30	2000 ± 70	1900 ± 50	1.3 ± 0.85	2.3 ± 0.15	9.3 ± 0.55	60
1.30	30 to 50	30 to 40	2050 ± 70	1850 ± 70	1.9 ± 0.15	6.2 ± 0.40	21.6 ± 1.25	80
2.60	40 to 50	30 to 50	2700 ± 70	2000 ± 70	3.3 ± 0.20	9.3 ± 0.75	23.2 ± 1.65	85
4.60	50 to 70	40 to 60	5010 ± 90	2250 ± 70	6.2 ± 0.45	16.3 ± 1.0	40.6 ± 4.05	95
6.80	to 70	110 to 130	7270 ± 90	2370 ± 70	9.0 ± 0.65	18.1 ± 1.15	58.3 ± 4.15	100
Steel C40								
0.52	10 to 15	10 to 20	2350 ± 70	2000 ± 70	1.6 ± 0.10	3.0 ± 0.20	8.1 ± 0.55	50
2.60	30 to 70	30 to 70	3500 ± 80	4500 ± 80	1.9 ± 0.15	4.1 ± 0.25	11.6 ± 0.75	70
6.80	60 to 130	130 to 150	7400 ± 90	2390 ± 70	8.1 ± 0.55	17.3 ± 1.25	49.0 ± 3.55	100

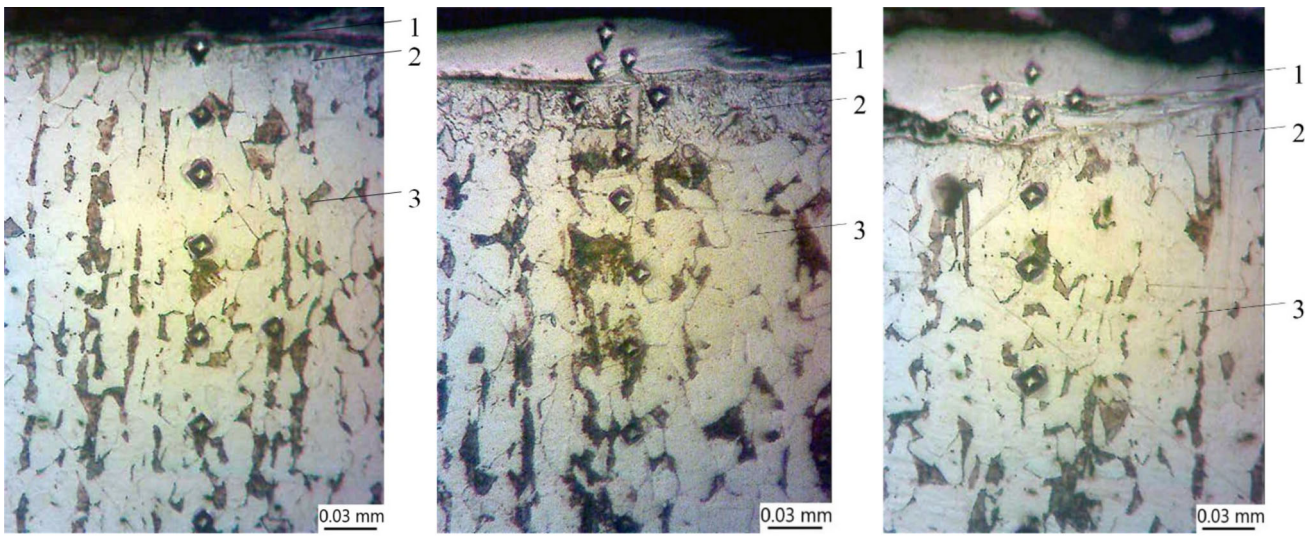

(a) (b) (c)

Fig. 3—Structure of the alitised coating (optical microscopy) on steel C20 after ESA at the discharge energy: (*a*) 0.52 J, (*b*) 1.30 J, and (*c*) 2.6 J. Areas of microstructure: 1: "white" layer, 2: diffusion zone, 3: substrate.

each specimen. Results are presented as mean values with standard deviation. X-ray diffraction studies were carried out in Cu Kα radiation using a PROTO AXRD diffractometer. The surface samples were prepared prior to X-ray diffraction analysis for roughness reduction.

IV. RESULTS

A. *Study of the Structure and Phase State of Aluminised Coatings at Traditional Productivity*

In order to evaluate the effect of the discharge energy on the surface quality, the morphology of the surface of the samples after the treatment was studied (Figure 2). The general shape of the elements of surface microroughness is uniform. A series of peaks and valleys can be identified on the surface, the geometric dimensions of which depend on the treatment regime. A significant increase in micro-irregularities on the surface of the sample is observed after ESA at W_p = 2.6 J, which is associated with the localisation of the discharge flow and the uneven distribution of the transferred substance with an increase in the energy impact.[44] The values of the surface roughness depending on the energy parameters of the treatment are presented in Table III.

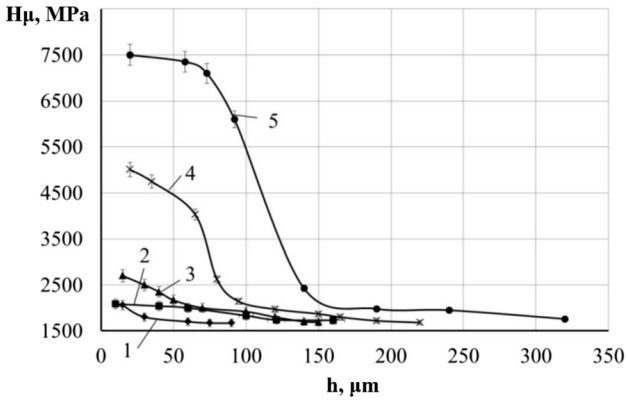

Fig. 4—Distribution of microhardness (H_μ) in the aluminised coating (h) on steel C20 during ESA with discharge energy: 1: 0.52 J, 2: 1.30 J, 3: 2.6 J, 4: 4.6 J, 5: 6.8 J.

The microstructure of the alitised surface of steel C20 depending on the discharge energy and at traditional productivity (Table I) is presented in Figure 3. The results of the optical microscopy show that the microstructure is composed of three areas:

(1) "white" layer that does not get etched when exposed to the reagent;
(2) diffusion zone;
(3) substrate, which has a ferrite-pearlite structure characteristic of annealed steel C20.

In the ESA process, a layer of modified structure is formed on the surface of the anode and cathode. When exposed to chemicals used to identify the microstructure of electrode materials, this layer remains "white", *i.e.*, its structure is not detected. Similar layers have been observed on the surfaces of materials subjected to mechanical processing (grinding, turning, milling, electromechanical processing), surface hardening processes (*e.g.*, shot treatment) and surfaces exposed to concentrated energy flows (laser, plasma, detonation, electric spark treatment, *etc.*).[20,22,32]

The formation of "white" layers under conditions of locally high temperatures and pressures is a common feature of all these cases. The intensity of the impact on the surface layer differs significantly from the above processes (shock wave pressure of 0.1 Pa, temperature of 5 °C to 40 × 10^3 °C). The high rate of heat removal causes the temperature to drop rapidly to melting temperatures and the associated phase transformations within a layer thickness of a few microns. The crystallisation, phase transformation, diffusion and chemical interactions involved in the ESA process lead to the

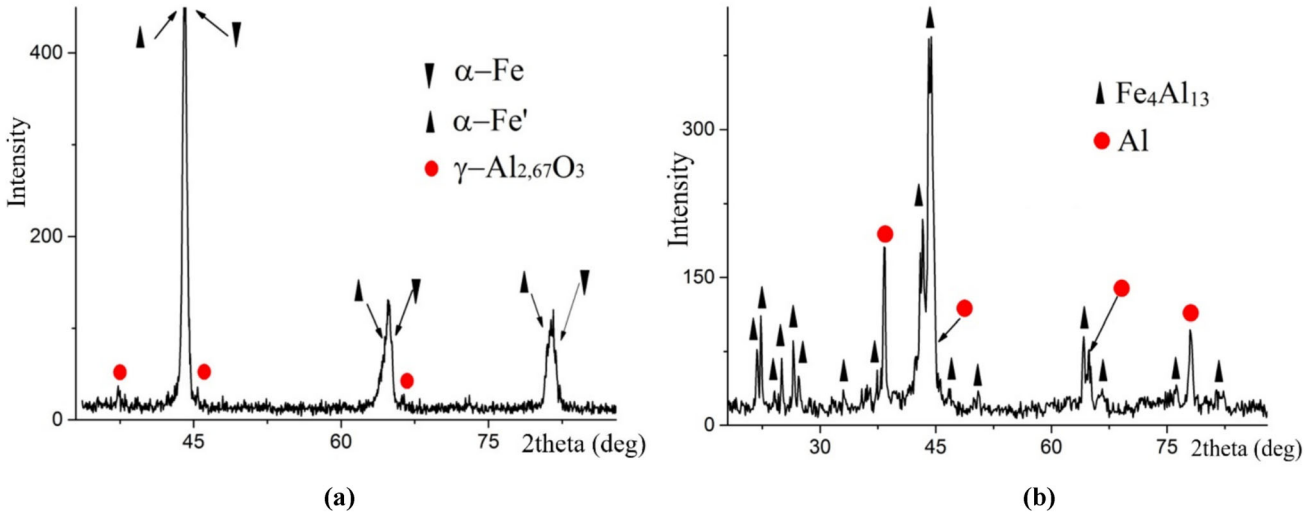

Fig. 5—Diffractograms of coatings on steel 20 after ESA alitisation at discharge energies: (*a*) 0.52 J, and (*b*) 1.30 J.

formation of highly non-equilibrium structures with very fine grain size and high heterogeneity in composition, structure and properties. The hardness of such a layer is usually much higher than that of the electrode materials. It is subject to stresses that exceed the internal stresses in the electrode materials of the anode and cathode.

The parameters of the microstructure sections formed as a function of the discharge energy of the ESA process are summarised in Table III.

In mode 1 ESA (Table I), a thin layer of the transition zone is formed with a thickness of 20 ÷ 30 μm. The continuity of this layer is close to 100 pct. Areas of the ''white'' layer (up to 60 pct) with a thickness of 10 ÷ 12 μm are detected. As the discharge energy increases, the thickness of the 'white' layer and the transition zone grows. At W_p = 1.30 J, the thickness of the cured layer and the transition zone are 30 ÷ 50 and 30 ÷ 40 μm, respectively, and at W_p = 4.60 J: 50 ÷ 70 and 40 ÷ 60 μm, respectively (Table III). As the W_p increases, the integrity of the coating improves. Thus, at W_p = 2.60 J, the continuity of the diffusion layer is about 100 pct and that of the ''white'' layer is about 85 pct.

The results of the microhardness distribution along the depth of the alite layer are shown in Figure 4. It should be noted that the maximum hardness is fixed at the surface and gradually decreases to the substrate, whose microhardness is 1600 ÷ 1700 MPa. A gradual change in the microhardness of the coating (1 to 4 on Figure 4) substrate indicates a good adhesion–diffusion bond between the coating and the substrate. In coarse modes, a higher change in microhardness is observed at the coating–substrate interface due to stresses in the surface layer[45] (5 on Figure 4). The microhardness of the coating zones is determined by the energy parameters of the ESA: the more energy the discharge, the higher the hardness of the 'white' layer and, accordingly, the hardness of the diffusion zone. The change in microhardness is probably caused by diffusing aluminium into the substrate and is also caused by changing the phase composition of the coating.

According to the diagram of the Fe–Al state,[46] the formation of intermetallic compounds is possible in the alitised coating synthesised by the ESA method. The formation of nitrides and oxides is also likely as ESA was carried out in an air environment. Deposition of the electrode material, aluminium, on the surface of the treated material is also possible.

The conditions of the phase composition formation during ESA are far from equilibrium.[16] This is due to the heating and cooling conditions. There are rapid heating and cooling in ESA. During cooling, the temperature rapidly decreases from the melting point to the phase transformation temperature. In this context, metastable phases are formed during ESA, and it is possible to form a nanostructure[45] and an amorphous structure.[48] The phase composition is also influenced by other factors, such as the chemical interaction of the electrode materials with each other and with the interelectrode medium, different erosion resistance of the alloy electrode components, and more.[48] Studies of the regularities in the formation of the structure and phase composition of electrospark coatings have shown that, despite the simplicity of the technology, ESA is a complex and multivariate process.

The phase composition of the coatings formed after the ESA process is determined. Diffraction patterns (Figure 5) from the surface of the samples after ESA according to the modes in Table I. The diffraction peaks of two solid solutions with BCC structure—α-Fe and α-Fe′ (space group 229), aluminium oxide γ-$Al_{2.67}O_4$ (space group 227) appear in the diffraction diagrams. Table IV shows the lattice parameters of the phases. According to Reference 41, the only difference between the α-Fe phases and the α-Fe′ phases is in the lattice period. The difference in lattice parameters is due to the macrostresses that occur during accelerated cooling after ESA.

The phase composition of coatings is significantly affected by the discharge energy. New phases appear as the discharge energy increases. If in Regime 1 only a solid solution of aluminium in iron and a small amount of aluminium oxide is detected, because the ESA was carried out in an air atmosphere, then in Regime 2 phases with a monoclinic structure are formed, namely Fe_4Al_{13} (space group 12) and aluminium is deposited (space group 225). It is obvious that the hardness of the coating is increased (Figure 4) by the appearance of intermetallic phases of more than 80 pct by mass.

We have shown, as have the authors of References 22, 30, 49, that an increase in discharge energy leads to a growth in the thickness of the coating and the diffusion zone. The thickness of the diffusion zone of aluminium in iron is 34 and 50 μm, respectively, on the samples obtained in regimes 1 and 2 (Figure 6). It should be noted that the amount of aluminium in iron also

Table IV. Phase Composition and Phase Lattice Parameters

Regime	Phase	Crystal Lattice Parameters (nm)	Content of Phases, Pct (Wt)
1	α-Fe	a = 0.2887	36
	α-Fe′	a = 0.2907	47
	γ-$Al_{2,67}O_4$	a = 0.7980	17
2	Al	a = 0.4056	19
	Fe_4Al_{13}	a = 1.5403, b = 0.8134, c = 1.2473	81

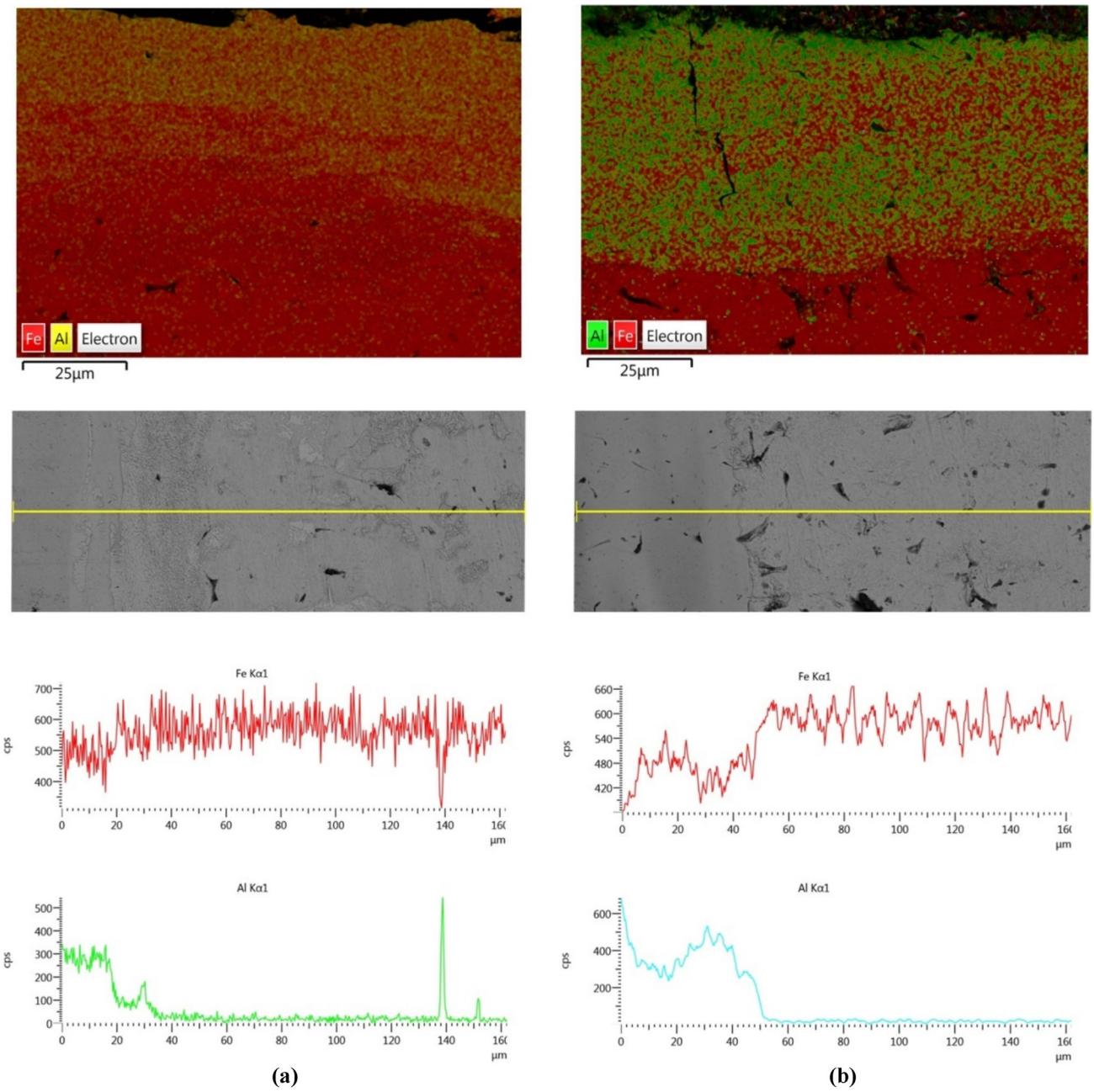

Fig. 6—Element distributions in the alitised coating at ESA with discharge energy: (*a*) 0.52 J, and (*b*) 1.30 J.

increases: at a discharge energy of 1.30 J, a layer (up to 4 μm) containing ~ 1.5 to 2 times more aluminium is formed on the surface of the sample. XRD data (Table IV) confirm the presence of free aluminium in the layer.

The study of the roughness of the modified surface after alitisation by the ESA method of steel C20 showed that as the discharge energy increases, the surface quality deteriorates (Table III): Ra = 1.3 μm at W_p = 0.52 J and Ra = 3.3 μm at W_p = 2.60 J. Increasing the discharge energy to 6.8 J is accompanied by a significant rise in surface roughness: R_{max} = 58.305 μm, Ra = 9.039 μm and R_z = 18.142 μm.

Optical microscopy results of samples of steel C40 after ESA metal treatment show that, similar to steel C20, the coating consists of several zones. It should be noted that in the same ESA conditions on steel C40, the thickness of the hardened 'white' layer and the diffusion zone is slightly greater (Table III). These areas also have a higher microhardness. For example, the coating obtained on steel C40 in regime 3 has a white layer thickness of 30 ÷ 70 μm and H_μ = 3500 ± 50 MPa, and on steel C20 in the same regime 40 ÷ 50 μm and H_μ = 2700 ± 70 MPa. Coating continuity improves and tends to 100 pct as the discharge energy increases.

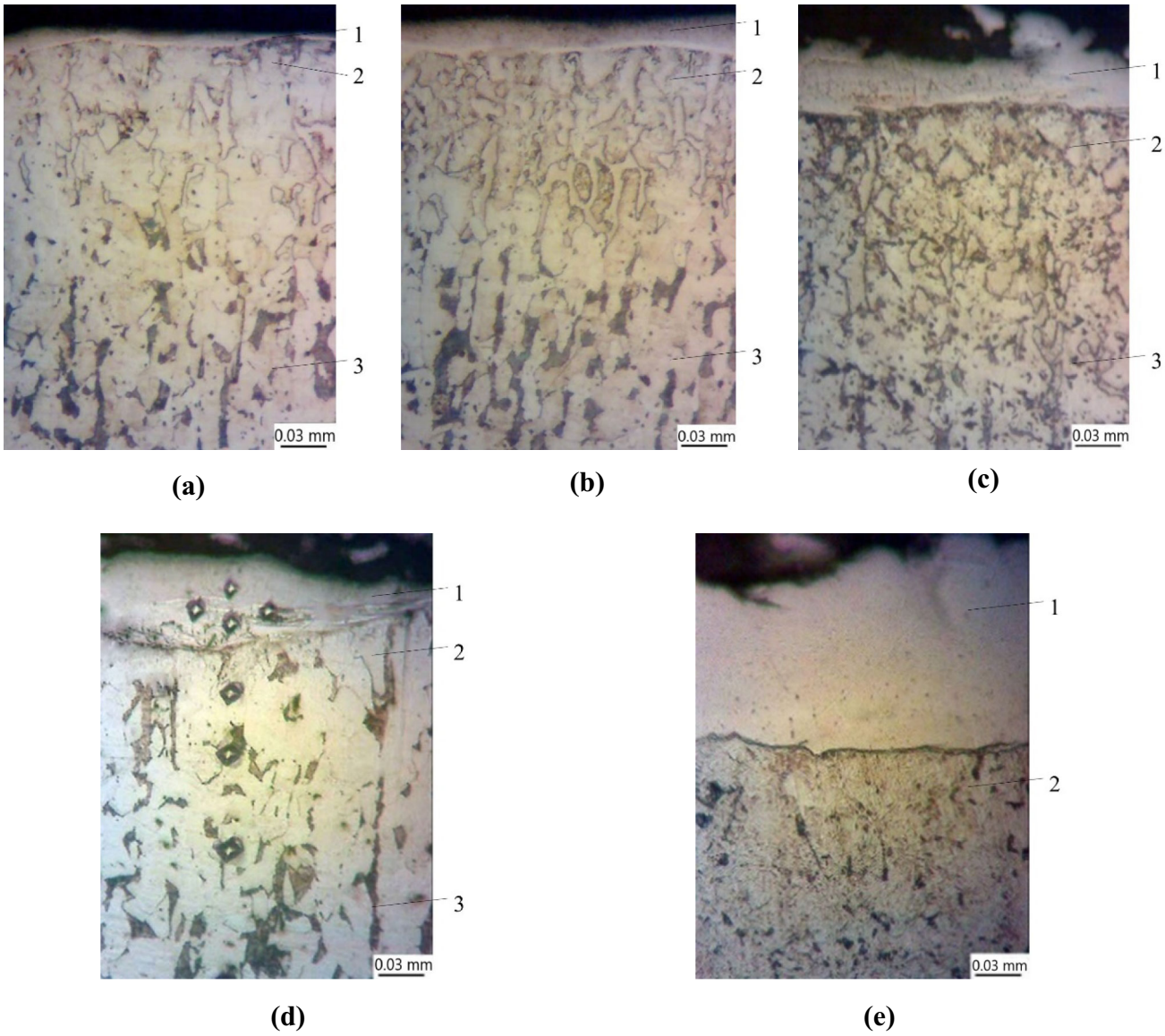

Fig. 7—The structure of the alitised coating on steel C20 after ESA with reduced productivity (1st option, Table II) and discharge energy: (*a*) 0.52 J, (*b*) 1.3 J, (*c*) 2.6 J, (*d*) 4.6 J, and (*e*) 6.8 J. Areas of microstructure: 1: "white" layer, 2: diffusion zone, 3: substrate.

Higher discharge energy accelerates the diffusion processes during ESA, and obviously the diffusion zone between coating and substrate grows. For example, at $W_p = 0.52$ J it is practically non-existent, whereas at $W_p = 2.60$ J it is about $30 \div 40$ μm and has an elevated microhardness (4500 MPa). Phase transformations that occur when steel is heated above critical temperatures and accelerated cooling in air can cause the increase in hardness in the transition zone. Some hardening of the surface layer of the steel results from the accelerated cooling after ESA. Similar to steel C20, intermetallics, nitrides and oxides can form in the surface layer of steel C40. This is due to the fact that the ESA process was carried out in air. The formation of these phases helps to increase the microhardness of the coating and the diffused zone.

Thus, qualitative parameters of the surface layer such as roughness, thickness, microhardness of the 'white' layer and transition zone rise with increasing discharge energy during ESA with an aluminium electrode of steel C20 and C40. The continuity of the "white" layer is low at $W_p = 0.52$ J and amounts to $50 \div 60$ pct. When the discharge energy is further increased to 6.8 J, it grows to 100 pct.

B. *Study of the Structure and Phase State of Aluminised Coatings at Reduced Productivity*

1. *The first option*

The microstructure of coatings produced by electro-spark alloying (ESA) with an aluminium electrode varies significantly depending on the treatment parameters, in

Table V. Qualitative Parameters of the Surface Layers of C20 Steel Samples After ESA with an Aluminium Electrode According to the Second Method

Discharge Energy (J)	Productivity (cm^2/min)	Thickness (μm)		Maximum Microhardness (MPa)		Roughness (μm)			Continuity of the "White" Layer (Pct)
		"White" Layer	Transition Zone	"White" Layer	Transition Zone	Ra	R_z	R_{max}	
ESA Productivity According to Table II, First Option									
0.52	0.5 to 0.6	20	35	2200 ± 50	1950 ± 50	1.1 ± 0.05	2.1 ± 0.15	8.7 ± 0.75	80
1.30	0.6 to 0.7	50	50	2250 ± 50	1950 ± 50	2 ± 0.15	5.1 ± 0.30	16.3 ± 0.95	90
2.60	0.7 to 1.0	60	55	2900 ± 70	2100 ± 50	3.8 ± 0.20	6.3 ± 0.35	19.6 ± 1.35	95
4.60	1.0 to 1.2	70	70	5300 ± 70	2350 ± 50	6.2 ± 0.45	12.1 ± 0.85	33.1 ± 2.35	100
6.8	1.2 to 1.5	75	120	7400 ± 90	2400 ± 50	9.0 ± 0.55	15.4 ± 0.95	45.2 ± 2.65	100
ESA Productivity According to Table II, Second Option									
0.52	0.2 to 0.3	25	40	2250 ± 50	1980 ± 50	1.3 ± 0.05	2.0 ± 0.15	8.5 ± 0.75	95
1.30	0.3 to 0.4	50	55	2300 ± 50	2000 ± 50	2 ± 0.15	6.1 ± 0.35	15.6 ± 1.25	100
2.60	0.4 to 0.5	57	60	2950 ± 50	2050 ± 50	3.8 ± 0.25	9.1 ± 0.60	18.1 ± 1.10	100
4.60	0.5 to 0.6	60	80	5300 ± 70	2000 ± 50	6.2 ± 0.40	16.0 ± 0.95	31.2 ± 2.35	100
6.8	0.6 to 0.7	60	100	7300 ± 90	2150 ± 50	9.0 ± 0.50	18.1 ± 1.25	43.3 ± 2.45	100

Table VI. Qualitative Parameters of the Surface Layers of C40 Steel Samples After ESA with an Aluminium Electrode According to the Second Method

Discharge Energy (J)	Productivity (cm^2/min)	Thickness (μm)		Maximum Microhardness (MPa)		Roughness (μm)			Continuity of the "White" Layer
		"White" Layer	Transition Zone	"White" Layer	Transition Zone	Ra	R_z	R_{max}	
ESA Productivity According to Table II, the First Option									
0.52	0.5 to 0.6	25	40	2400 ± 50	2100 ± 50	1.0 ± 0.05	3.0 ± 0.25	6.2 ± 0.50	60
2.60	0.7 to 1.0	70	80	3650 ± 50	4600 ± 50	1.9 ± 0.15	4.1 ± 0.25	8.6 ± 0.65	90
6.8	1.2 to 1.5	110	140	7450 ± 70	2490 ± 50	8.1 ± 0.55	17.3 ± 1.05	42.1 ± 2.85	100
ESA Productivity According to Table II, the Second Option									
0.52	0.2 to 0.3	30	45	2450 ± 50	2130 ± 50	1.6 ± 0.05	3.0 ± 0.25	6.1 ± 0.55	95
2.60	0.4 to 0.5	70	80	3650 ± 50	4650 ± 50	1.9 ± 0.15	4.1 ± 0.30	7.7 ± 0.60	100
6.8	0.6 to 0.7	100	130	7300 ± 70	2030 ± 50	8.1 ± 0.60	17.3 ± 1.15	39.1 ± 2.75	100

particular the discharge energy (W_p) and the productivity. In all ESA regimes, the structure of the alloyed layer consists of a 'white' layer, a diffusion zone and a substrate material (Figure 7). The parameters of these layers are determined by the treatment conditions (Tables V and VI).

As the discharge energy is increased from 0.52 to 6.8 J, an rise in the thickness of the 'white layer' and the diffusion zone is observed—from 20 to 75 and from 35 to 120 μm, respectively. Such patterns are in agreement with the data from the literature, according to which a more intense pulse effect promotes a deeper melting of the substrate material and a deeper penetration of the alloying element.[44,45] Coating continuity also improves with increasing discharge energy, reaching almost 100 pct at $W_p \geq 2.6$ J. This is due to the fact that at higher discharge energy a wider zone of impact is formed on the surface, ensuring better wettability of the substrate by the aluminium. As noted in Reference 50, the continuity of coatings is closely related to the formation of repeated layers, which partially melt and level the previously applied material.

With regard to the effect of the alloying time, *i.e.*, a reduction in the productivity of the treatment, an increase in the thickness of the "white layer" and the diffusion zone is observed in comparison with the classical values (Table III). As the alloying time increases, the period of exposure to elevated temperature rises, diffusion processes are activated, leading to the formation of a homogeneous structure with fine-grained phases formed under conditions of accelerated cooling in air. Such processes can have a positive effect on the adhesion of the coating, as slower crystallisation hardening and longer contact of the melt with the substrate contribute to deeper diffusion interpenetration of the components.

A reduction in ESA productivity has a positive effect on surface roughness (Tables V and VI). With a longer treatment time per unit area, the tool electrode makes more passes over the same surface area, which leads to re-melting of the deposited layer and filling of microcavities with aluminium. This is corroborated by studies showing the effect of levelling the microrelief due to heat accumulation and re-melting of low-melting phases.[51]

Figure 8 shows the microhardness test results of the surface layers obtained by the second method. It shows that as the discharge energy higher, the microhardness of the surface layer increases, both in the 'white' layer and in the transition (diffusion) zone. Thus, as the energy rises, the zone of higher microhardness increases. The maximum microhardness is observed at the surface of the formed layers. It gradually decreases from the surface to the substrate.

ESA hardening is associated with the formation of non-equilibrium structures in the surface layer during heating and cooling.[48] The high rate of heat dissipation causes the temperature within a small layer to drop rapidly to melting temperatures and corresponding phase transformations. In this case, the crystallisation and phase transformations that follow the ESA treatment lead to the formation of highly non-equilibrium structures with very fine grains, high levels of heterogeneity in composition, structure and properties.[52] Ultra-high heating and cooling rates, contact of juvenile surfaces with each other and with medium elements under conditions of impulse exposure to high temperatures and pressures, high rate of diffusion processes leading to chemical interaction of electrode materials with the medium, *etc*. cause the appearance of ESA layers with increased values of microhardness.

An analysis of the influence of the substrate material, steel C20 and C40, showed that the changes in the microhardness increase both in the white layer and in the transition (diffusion) zone are insignificant (see Tables V and VI).

2. *The second option*

Figure 9 shows different sections of the surface structure of samples of steel C20 after ESA with an aluminium electrode at a factor 4 reduced productivity (ESA modes 2nd option, Table II). Tables V and VI summarise the data on the quality parameters of the coatings for steel C20 and C40, respectively. It should be noted that the characteristics of the microstructure do not change with decreasing productivity. The coating consists of a 'white' layer on the surface, a diffusion zone and the substrate material. At the same time, the continuity increases to 100 pct at almost any discharge energy. The thickness of the 'white' layer and the diffusion zone increases from 25 to 60 and 40 to 60 μm, respectively, with rising W_p from 0.52 to 2.6 J, then remains practically unchanged at W_p = 4.6 J and even decreases at W_p = 6.8 J.

The surface roughness with a decrease in the productivity of ESA (using the 2nd option) decreased slightly in relation to the value of the roughness, which corresponds to the productivity indicated in Table II for the 1st option. As the productivity of the ESA process is lowered, the processing time for 1 cm^2 of surface area increases. The crystallisation of each subsequent layer is slower due to the heat accumulation of the low-melting metal (aluminium) melt. However, the roughness reduction process is not as intense. This can be explained by the fact that with each successive "pass" of the aluminium electrode tool, the difference between the amount of aluminium and steel in the coating becomes smaller.

The microhardness distribution in the surface layers obtained by the second method is shown in Figure 10. It can be seen that the coating has a well developed diffusion zone. The microhardness gradually decreases from the surface to the substrate. As with other ESA regimes, the increase in microhardness is associated with the peculiarities of structure-phase transformations and the formation of a non-equilibrium state in the surface layer.

Analysis of the results showed that a 4-fold reduction in productivity has a negative effect on the quality indicators of aluminised coatings. Irrespective of the substrate material, treatment at low energies (0.52 to 2.60 J) leads to a slight change in microhardness and coating thickness, and at rough conditions (4.60 to 6.8 J) even to a deterioration of these parameters compared to other treatment methods. The reason for these results seems to be related to the peculiarities of the ESA technology.

It should be noted that although a 4-fold reduction in productivity results in a moderate increase in surface roughness (Tables V and VI), the continuity is significantly improved, reaching 100 pct. This is explained by the mechanism of coating formation at low productivity. The longer treatment time allows a more uniform and repeated deposition of the electrode material (aluminium), which contributes to the gradual filling of microcavities and surface irregularities, remelting of the deposited material and compaction. As a result, even if the surface becomes rougher due to the larger size of the solidified droplets during ESA under more severe ESA conditions (discharge energy of 2.6 J and above), the overall coating becomes more continuous. In addition, the high thermal impact at reduced productivity increases local melting and spreading of the material, which contributes to improved adhesion and sealing of microdefects. However, a significant reduction in productivity in the coarse W_p mode increases the thermal impact on the coating and diffusion zone, which reduces their microhardness. The increase in the roughness of the treated surface complicates the technological process of hardening parts under manufacturing conditions, since it is necessary to apply methods to reduce roughness. For example, cutting, surface plastic deformation and others.[31,53] Therefore, the increased productivity of the ESA process is ineffective in practice.

Dependencies of changes in quality parameters: 'white layer' thickness, microhardness and surface roughness of steel C20 were constructed to evaluate the influence of ESA operating parameters (discharge energy and productivity) (Figures 11 and 12). The formation of a continuous aluminised layer on steel C20 is observed at discharge energies < 4.6 J and productivity < 1.0 cm^2/min for the first treatment option and < 1.3 J and productivity < 0.3 cm^2/min for the second treatment option. The coating thickness is < 70 μm. Thus, a reduction in the productivity by two times of the ESA has a positive effect on the quality characteristics of the aluminised layers, ensuring the formation of continuous

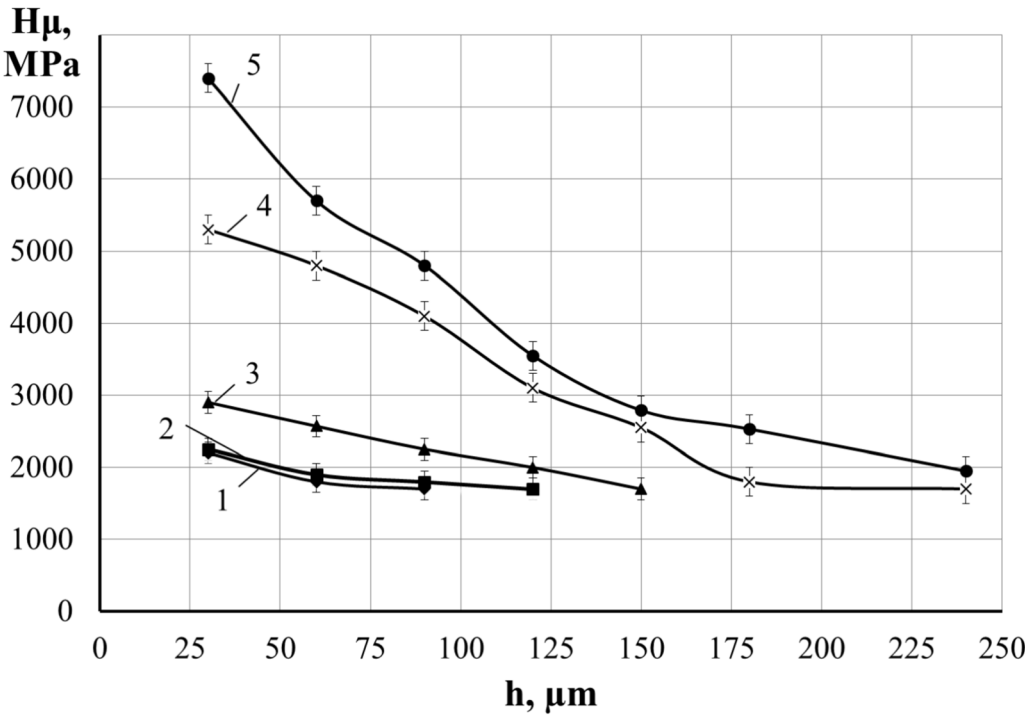

a

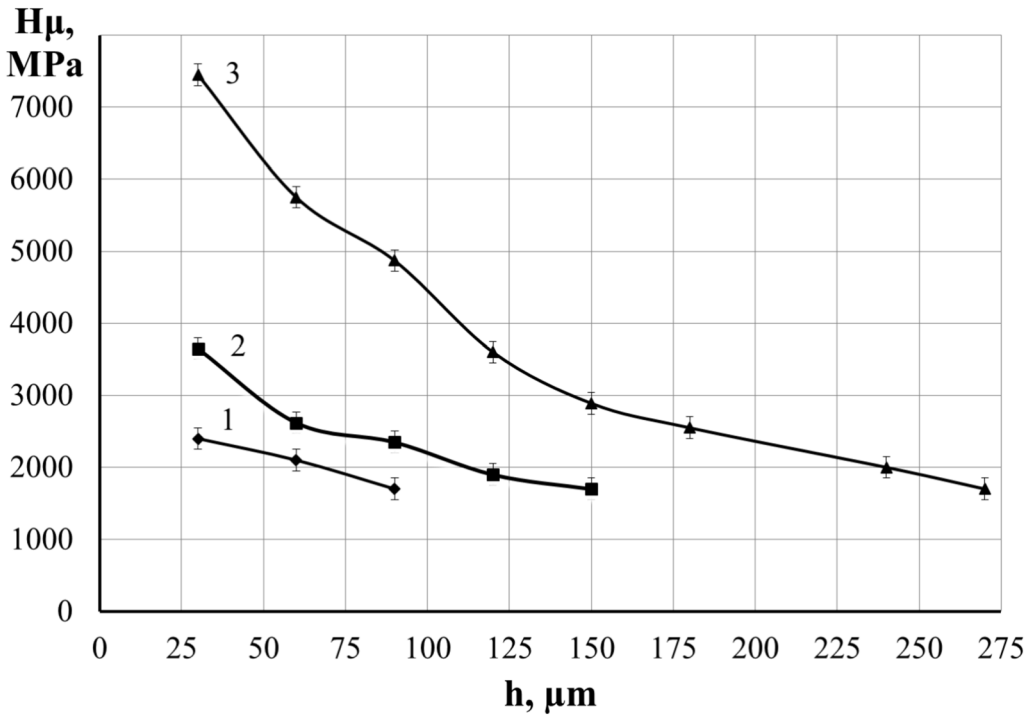

b

Fig. 8—Distribution of microhardness in the surface layer of steel C20 (*a*) and steel C40 (*b*) after ESA with an aluminium electrode according to the second method (1st option, Table II), discharge energy: 1: 0.52 J, 2: 1.3 J, 3: 2.6 J, 4: 4.6 J, 5: 6.8 J.

coatings that can be recommended for use as heat resistant.

The results obtained in this study indicate that a decrease in productivity during electrospark alloying (increase in alloying time) leads to a notable increase in both the thickness of the aluminium coating and the underlying diffusion zone. According to metallographic studies, diffusion zone thicknesses of approximately 35 and 40 μm were observed for samples of C20 steel processed under the regimes W_p = 0.52 J and productivity 0.5 to 0.6 cm^2/min (first option) and productivity 0.2 to 0.3 cm^2/min (second option) (Table V). Compositional analysis using scanning electron microscopy coupled with energy dispersive X-ray spectroscopy (SEM–EDS) was carried out to further substantiate these findings. This allowed visualisation and quantification of the aluminium distribution over the surface and depth of the treated layers as a function of productivity at the same discharge energy. For samples treated at a productivity of 0.5 to 0.6 and 0.2 to 0.3 cm^2/min, respectively, diffusion zone thicknesses of approximately 45 and 60 μm (including coating) were observed (Figure 13).

By reducing the productivity of ESA, there is a tendency to increase the thickness of the aluminium diffusion zone. In particular, compared to the traditional processing mode at a discharge energy of W_p = 0.52 J (see Figure 6), a decrease in the inverse of the treatment time (*i.e.*, productivity) leads to an increase in the time of interaction between the electrode and the sample surface, which contributes to the formation of thicker layers with a higher aluminium content. This behaviour is due to the fact that longer exposure to discharge pulses creates conditions for deeper penetration of aluminium into the substrate, activation of diffusion processes and accumulation of the alloying element.

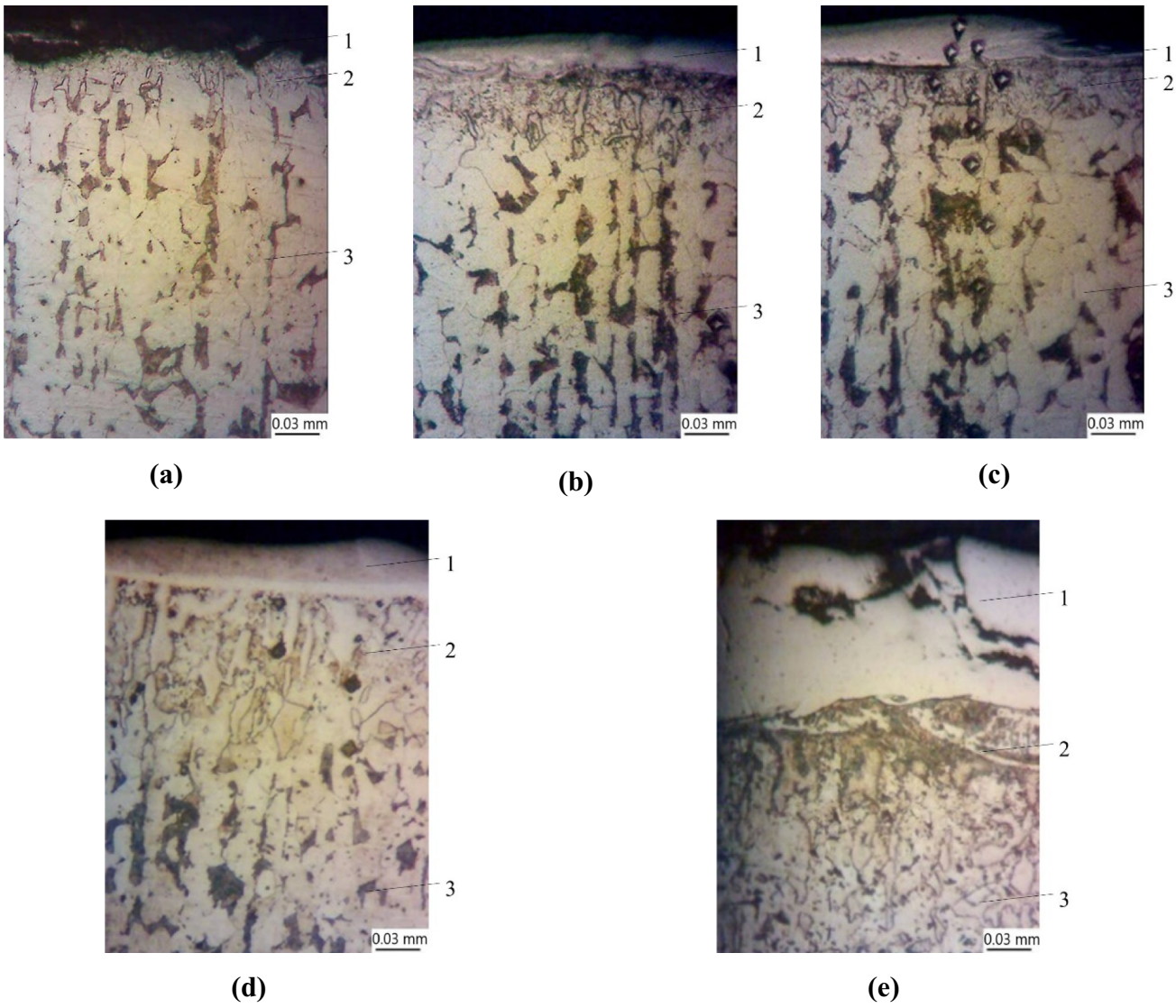

Fig. 9—The structure of the alitised coating (optical microscopy) on steel C20 after ESA with reduced productivity (2nd option, Table II) and discharge energy: (*a*) 0.52 J, (*b*) 1.3 J, (*c*) 2.6 J, (*d*) 4.6 J, and (*e*) 6.8 J. Areas of microstructure: 1: "white" layer, 2: diffusion zone, 3: substrate.

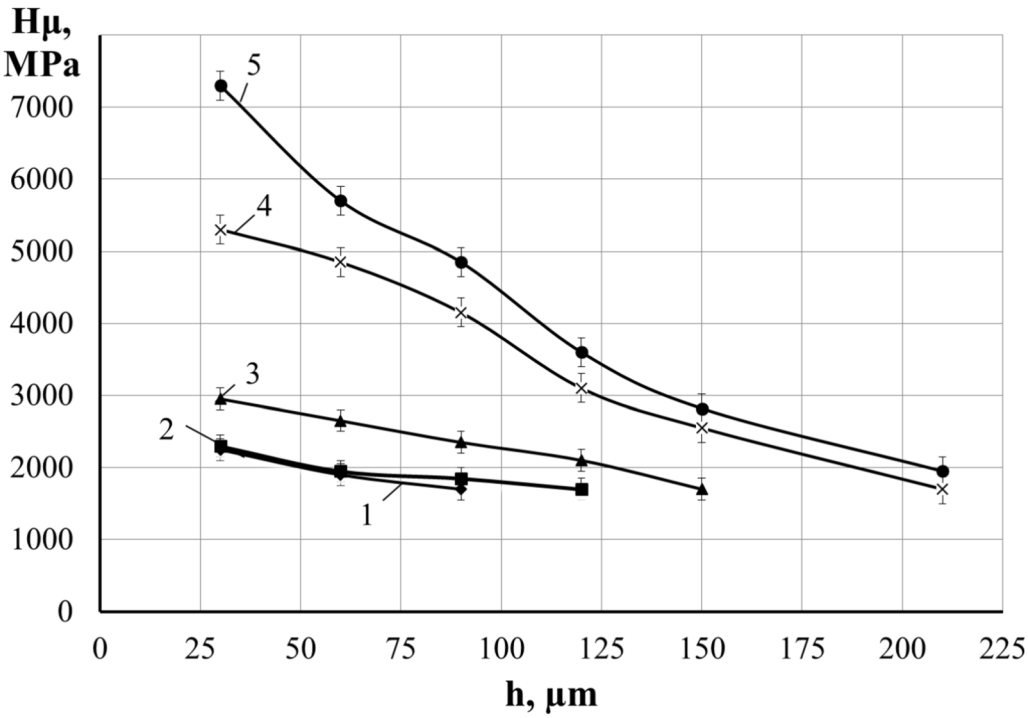

a

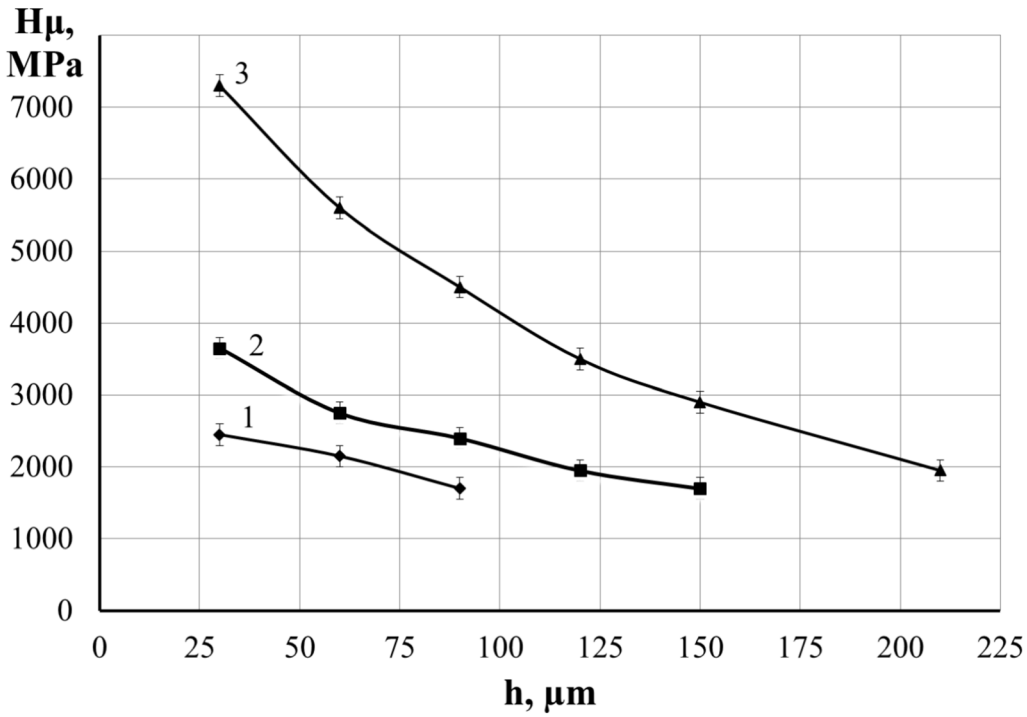

b

Fig. 10—Distribution of microhardness in the surface layer of steel C20 (*a*) and steel C40 (*b*) after ESA with an aluminium electrode according to the second method (2nd option, Table II), discharge energy: 1: 0.52 J, 2: 1.3 J, 3: 2.6 J, 4: 4.6 J, 5: 6.8 J.

In addition, the results of the analysis show that the aluminium is unevenly distributed in the coating. It is mainly concentrated near the surface. This localisation of enrichment leads to the formation of an aluminium-saturated surface layer. This is important for the subsequent properties of the coating, including its hardness, oxidation and corrosion resistance. Productivity control is therefore an effective tool for adjusting the thickness and chemical composition of coatings, allowing the penetration depth and concentration of the alloying element to be varied according to the requirements of the functional properties of the treated surface.

C. *Mathematical Model for Predicting the Quality Parameters of the Coating Produced by the ESA Method*

1. *Approaches to modelling*

The traditional method of assessing the efficiency of mass transfer from the anode to the cathode during electrospark alloying (ESA) is to study the change in electrode mass as a function of treatment time. Numerous experiments have shown that in most cases the cathode mass increases and the anode mass decreases at the initial moment of ESA.[22,54,55] At the same time, the absolute value of the decrease in the anode mass does not coincide with the increase in the cathode mass, which is explained by the fact that part of the substance is removed from the surface of both electrodes into the environment in the form of erosion products. After a certain processing time, the increase in cathode mass slows down and a decrease in cathode mass is observed. This behaviour is explained by the fact that, at different times of the ESA, two main competing processes contribute differently to the mass transfer: (1) an increase in the cathode mass due to polar mass transfer; (2) the destruction of the coating due to the accumulation of defects in it, the formation of brittle oxides and nitrides. First, there is a preferential transfer of material from the anode to the cathode, and then there is a greater loss of coating mass as a result of its destruction.

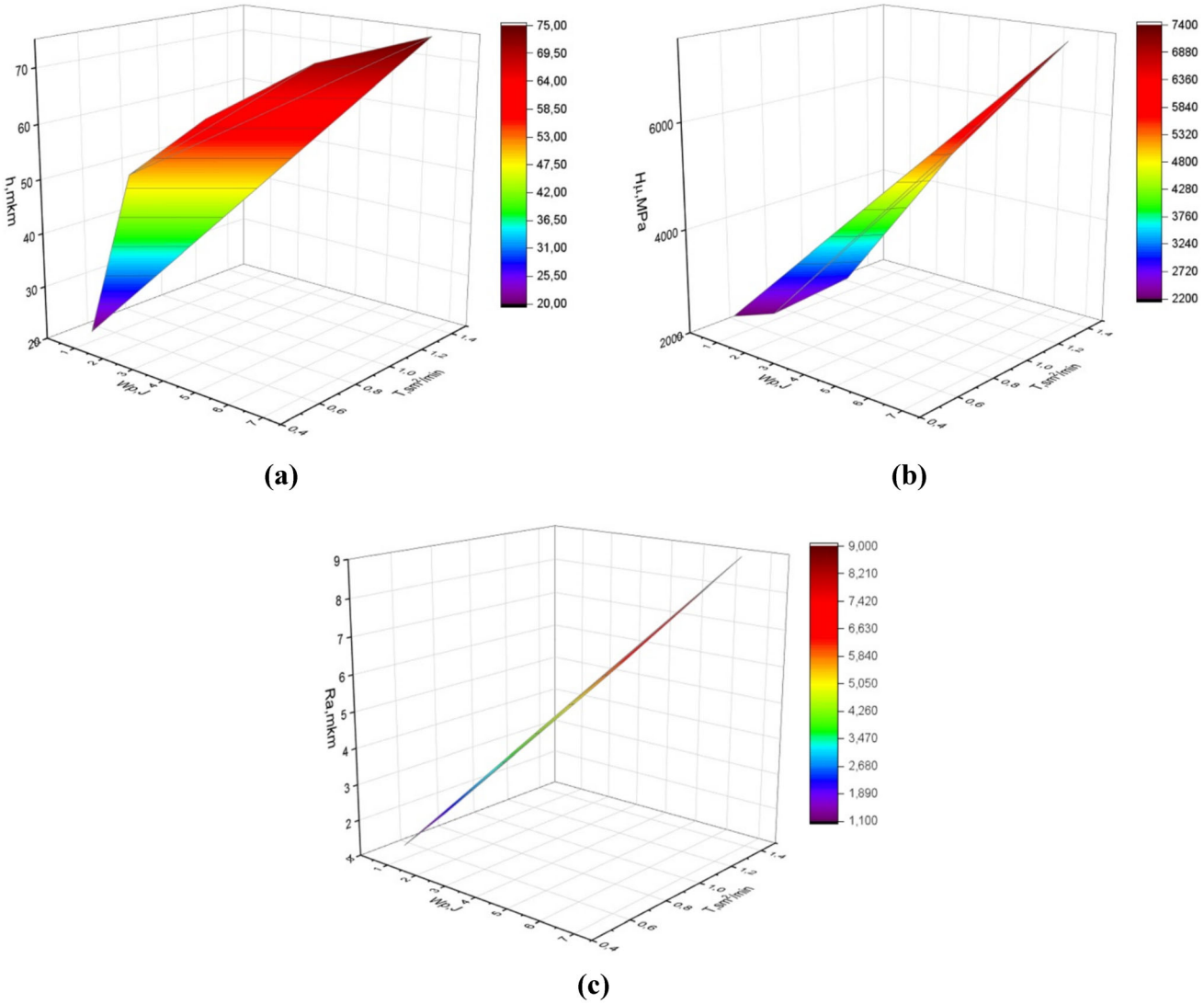

Fig. 11—Variation of quality parameters: thickness of 'white layer' (*a*), microhardness (*b*) and roughness (*c*) of surface layers of steel C20 as a function of discharge energy and ESA productivity (*T*) (according to the first option).

At present, there is a qualitative explanation of the mass transfer process during ESA, the theoretical description of the change in electrode mass remains open. This fact causes certain difficulties, since for each new electrode pair and processing mode, the kinetic dependencies of the electrode mass change have to be found experimentally.

The mass transfer coefficient TK, which is defined as the ratio of the change in cathode mass to the change in anode mass, *i.e.*, TK = $\Delta m_c/\Delta m_a$,[54] is often used to describe the mass transfer quantitatively.

Another indicator related to mass transfer is the thickness of the formed coating, which determines the quality of the coating and the life of the product. It is known[56] that in some cases 0.02 mm is sufficient to ensure high wear resistance of the surface layer of a part, for example in one-piece shaft–hub joints when the contacting surfaces of the parts are joined by tension, *i.e.*, the shaft diameter is larger than the hub diameter, and sometimes it is necessary to apply wear-resistant coatings with a thickness of 2.0 mm or more.

The values of the electrospark alloying parameters have a significant effect on the intensity of the coating process and the quality of the surface. The most important are the discharge power (energy) and the alloying productivity (time), *i.e.*, the area of surface treated per unit of time. The influence of electrical parameters (current, voltage, discharge energy, *etc.*) when using different electrode materials has been extensively studied.[22,36,56,57] An increase in discharge energy leads to an increase in the size of each individual electrical discharge and, within certain limits, contributes to an increase in the amount of coating material transferred and to deeper surface transformations in the discharge zone. The same applies to the process time, *i.e.*, the labour intensity (reverse productivity), which increases with the thickness of the layers applied.

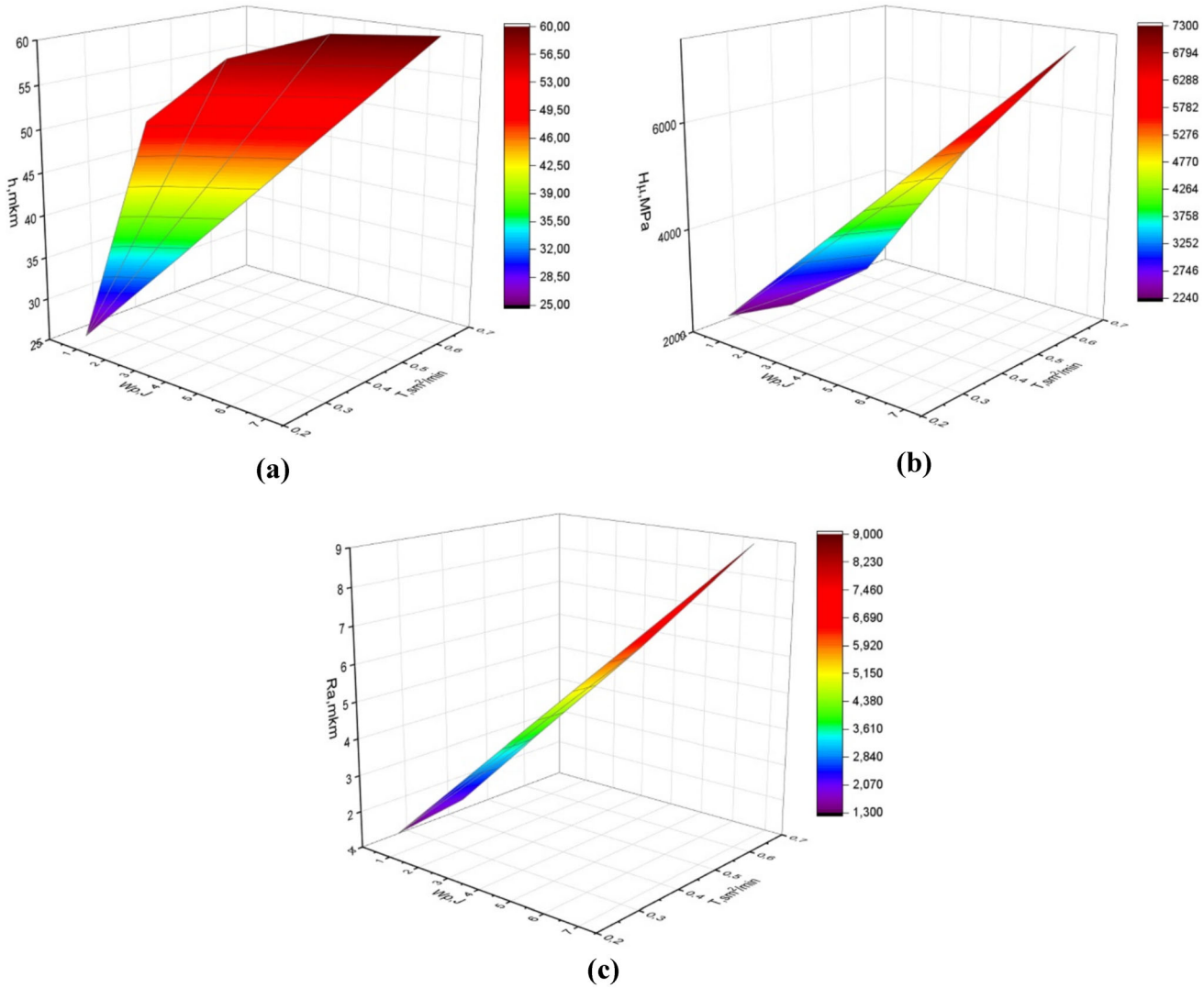

Fig. 12—Variation of quality parameters: thickness of 'white layer' (*a*), microhardness (*b*) and roughness (*c*) of surface layers of steel C20 as a function of discharge energy and ESA productivity (*T*) (according to the 2nd option).

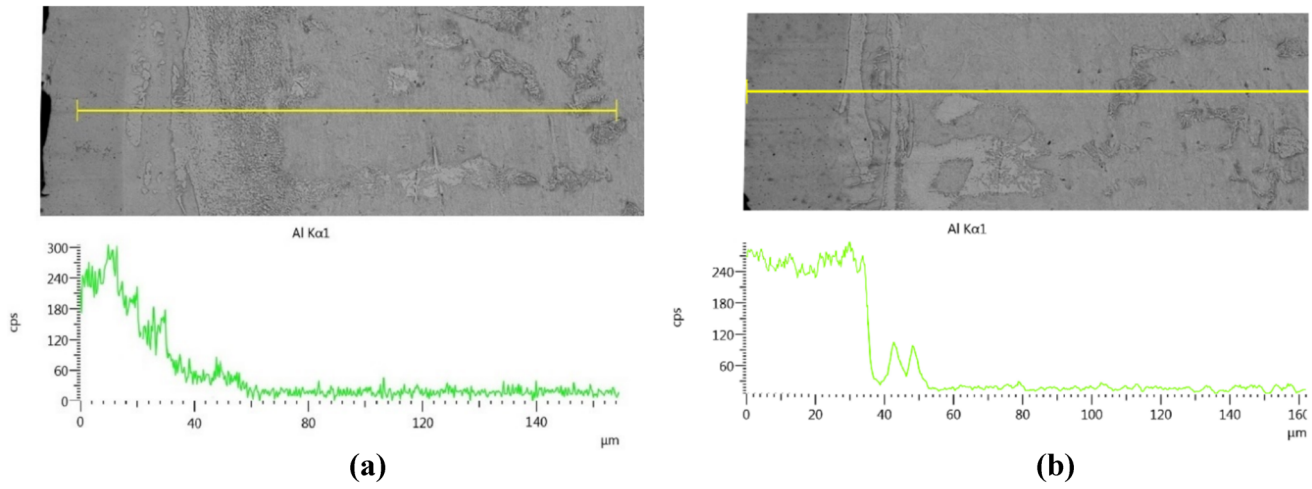

Fig. 13—Element distributions in the alitised coating on steel C20 at ESA with discharge energy 0.52 J and productivity (*a*) productivity 0.5 to 0.6 cm^2/min (first option), and (*b*) 0.2 to 0.3 cm^2/min (second option).

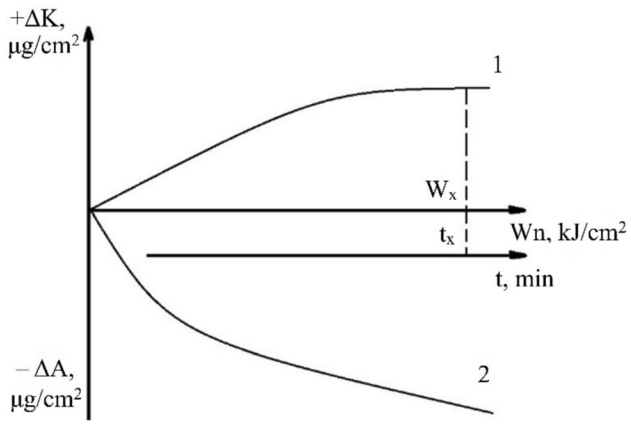

Fig. 14—Change in weight of cathode (1) and anode (2) as a function of applied energy and processing time. In the figure, ΔA is the specific erosion of the anode, ΔK is the cathode growth, W_n is the given value of the spark discharge energy when alloying a substrate with an area of 1 cm^2.

The main difficulty in using ESA in practice is the selection of the optimum specific alloying time. This is due to the non-linear change in the total weight gain of the sample during ESA. As can be seen from Figure 14, starting from the value of the brittle fracture threshold of the modified surface layer t_x, the total weight gain of the cathode becomes negative. By increasing the specific alloying time $t > t_x$, the sample weight can become less than the initial value. In general, an increase in sample weight with a change in t is only observed when $t < t_x$. This discrepancy is mainly due to the process of restoring parts, *i.e.*, achieving a predetermined increase in the linear size of the cathode. However, with regard to the surface hardening process in the manufacture of parts, where the increase in cathode weight should not be large and in some cases is not allowed, new methods of determining t_x are required. At the same time, the choice of t_x at different discharge energies, interelectrode media and alloying electrode materials is essentially the basis of ESA technology.[54,58]

In work,[59] it was experimentally established that the optimal doping time must be chosen for ESA τ_{opt}. It should be slightly less than or equal to the time τ_{max}, for which the maximum weight gain on the cathode is achieved, and less time τ_{br}, at where the reinforced layer begins to break down.

In addition, the duration of alloying at the selected alloying mode has virtually no effect on the roughness index, but determines the amount of material transferred from the anode to the cathode, the coating continuity and the coating thickness. By increasing the duration of the ESA, which ensures maximum mass gain on the cathode, the continuity and thickness of the coating will increase as the amount of material transferred rises.

A similar approach can be used to analyse changes in the thickness of the hardened layer (and/or diffusion zone), the continuity of the layer and its microhardness (Figure 15).

When changing the energy conditions of the alloying or the alloying time (productivity), it is extremely difficult to predict the direction of change in the structural and phase state of the coating. An increase in the total alloying time when using 1, 2,...,x alloying cycles leads to an increase in the duration of the thermal field, activation of diffusion processes, the possibility of phase transformations in the coating, *etc*. The conditions for crystallisation and cooling of the formed coating are also difficult to predict. In addition, the conditions for crystallisation and cooling of the formed layer change. Therefore, it can be assumed that with increasing cycles and changing alloying modes during repeated cycles, the hardness will change to a certain value.

With regard to the continuity (Figure 15(c)), if the value of 100 pct is not reached during the first alloying cycle, it tends to be reached during the subsequent cycles with ESA. This is obviously due to the fact that the treatment time for 1 cm^2 of surface area increases with

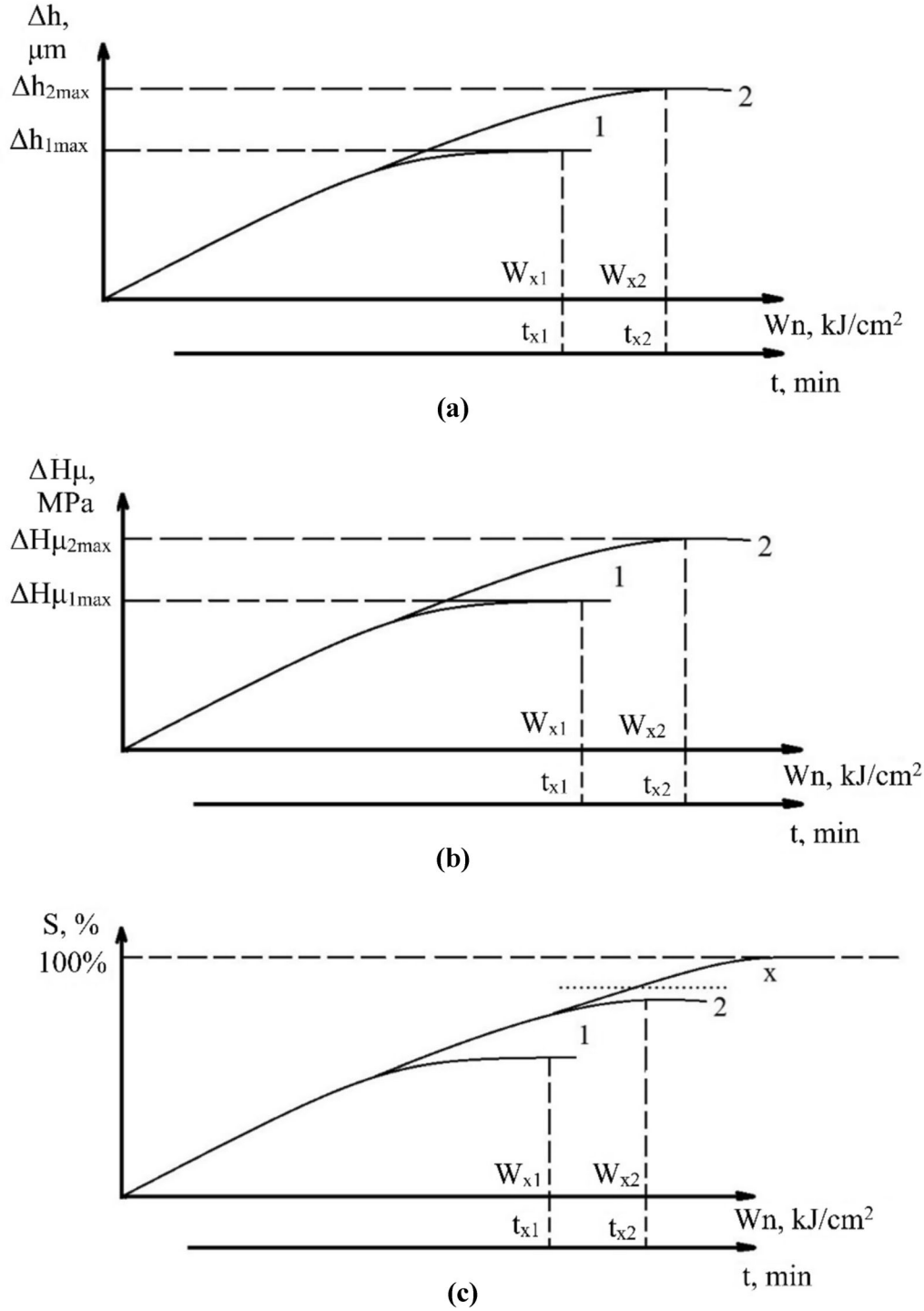

Fig. 15—Change in hardened layer thickness (*a*), hardness (*b*) and continuity (*c*) as a function of applied energy and treatment time.

the next treatment cycle. The number of ''passes'' of the tool electrode, and therefore the degree of reduction of the surface profile irregularities due to their melting and filling of the discontinuities, depends on the treatment time of each ESA cycle, *i.e.*, on the productivity of the process.

Therefore, the study of the influence of the energy parameters of ESA as well as the alloying time (productivity) of the process is important for the development of hardening technology. In order to reduce the number of experimental studies on the influence of different factors on the quality parameters of ESA coatings for a pair of electrodes, a mathematical model for predicting these parameters is needed, taking into

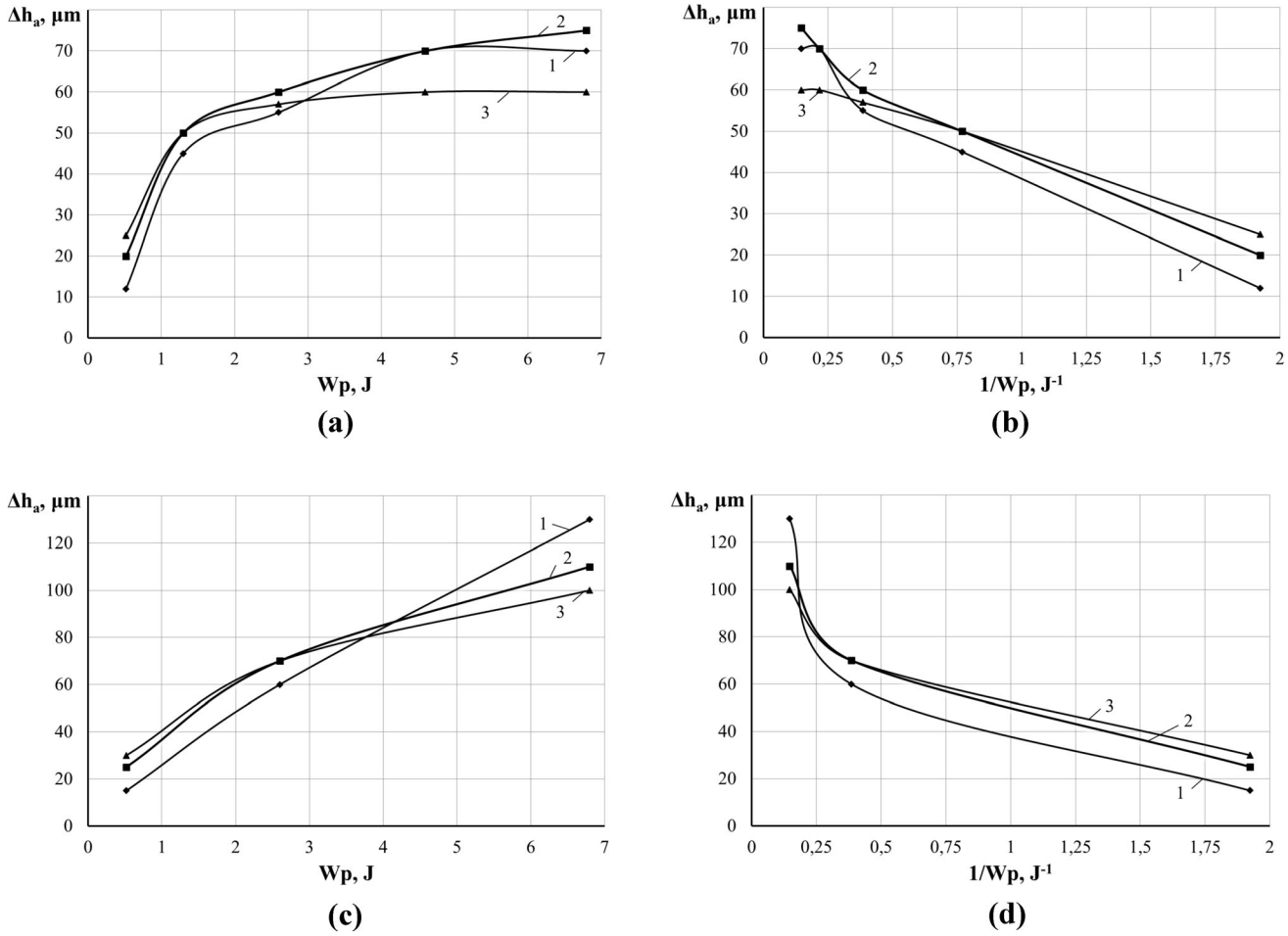

Fig. 16—Dependence of the thickness of the hardened layer during ESA alitisation of steel C20 (*a*, *b*) and steel C40 (*c*, *d*): a, c—on the discharge energy W_p; b, d—on the reverse discharge energy $1/W_p$. Graphs 1: traditional technology of ESA alitization; 2: productivity was reduced by about 2 factors (the 1st option, Table II); 3: productivity was reduced by about 4 factors (the 2nd option, Table II).

account the processing time of a given plane to be alloyed, *i.e.*, the labour intensity of the ESA process (the value of reverse productivity). Such a model will make it possible to control the surface properties of the parts.

2. *Mathematical Model Algorithm for Predicting Coating Quality Parameters Obtained by the ESA Method*

It is known[60] that the high adhesion between the coatings obtained by ESA and the substrate is explained both by the intensive mixing of the electrode materials in the liquid phase and by the diffusion of the anode material into the cathode in the solid phase. The diffusion processes are confirmed by the presence of a diffusion zone between the white layer and the substrate. This zone is not heated above the solidus temperature and does not interact directly with the environment. Therefore, its formation can be caused by the thermal effect of a pulsed discharge and the diffusion penetration of anode and cathode elements.

The diffusion coefficient is a temperature sensitive property (T). The diffusion coefficient D is given by the Arrhenius equation[61]:

$$D = D_0 \exp\left(-\frac{E_A}{RT}\right),$$

where E_A is activation energy of the diffusion process; R is the universal gas constant; T is temperature.

Such a dependence of the diffusion coefficient on temperature is experimentally confirmed for many systems with a high D value: for diffusion in interstitial (*e.g.*, carbon in α-Fe) and substitutional alloys (*e.g.*, gold in silver). The exponential dependence of D on temperature is an expression of the fact that diffusion occurs as a result of thermally activated movement of atoms, which is always described by an exponent $\exp\left(-\frac{q}{kT}\right)$, where q is the activation energy of the elementary act of moving the atom. In general, it will differ significantly for chemical elements and crystal structures. The activation energy can be estimated from the slope of the line that describes the dependence in coordinates lnD from the reverse temperature T^{-1}.

Studies of diffusion processes during electrospark alloying have shown that the depth of penetration of anode elements into the cathode during mass transfer in the solid phase can be several to one hundred

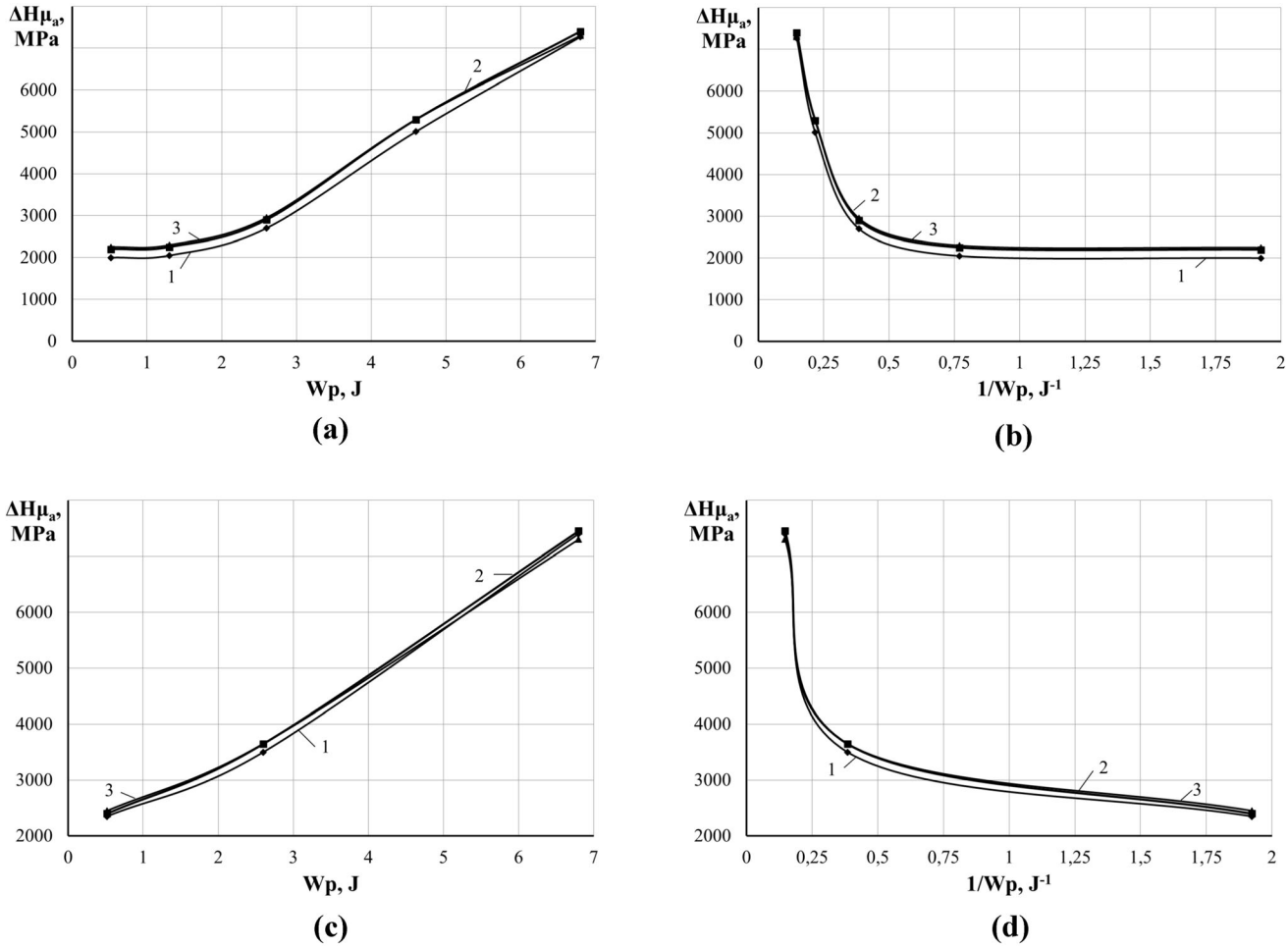

Fig. 17—Dependence of the microhardness of the hardened layer during ESA alitization of steel C20 (*a*, *b*) and steel C40 (*c*, *d*): a, c—on the discharge energy W_p; b, d—on the value of the reverse discharge energy $1/W_p$. In graphs: 1: traditional ESA aluminisation technology; 2: productivity was reduced by about 2 factors (the 1st option, Table II); 3: productivity was reduced by about 4 factors (the 2nd option, Table II).

micrometres or more, which has been repeatedly confirmed by metallographic and X-ray diffraction studies.[41,49,54,55,57,60,62] ESA results in irradiation, heating of the surface layer of the body and its plastic deformation, which distorts the lattice by forming point (vacancy and penetration atoms), linear and surface defects. In regular, defect-free structures, atoms are arranged in a lattice to form a system with minimum free energy. Displacement of atoms from their equilibrium position perturbs the lattice order. Energy is expended to create such perturbations, which is stored in the resulting defects. The value of the total energy of the system will be greater than the minimum energy characteristic of an ordered system of atoms by the amount of stored energy, which is determined by the number of defects in the lattice, their type, and is a kind of measure of the lattice defectivity.

It should be noted that the heating temperature of the cathode (the treated surface) depends on the discharge energy (W_p) at which the ESA process takes place. The existence of a directly proportional dependence indicates that as the discharge energy increases, the diffusion coefficients of the anode material elements into the substrate rise, and consequently the process efficiency. In this respect, the dependence of the thicknesses of the 'white' layer and the diffusion zone, as well as the diffusion coefficients, obey the exponential dependence (according to the Arrhenius equation).

On the basis of experimental studies, it was established that during alitization by the ESA method of steel C20 (Figures 8 and 10) with an increase in the discharge energy, the thickness of the strengthened layer rises (h_a, μm). Indicator h_a is complex, and consists of an growth due to an increase in discharge energy and a decrease in productivity.

Between values h_a and the reverse energy of the discharge (W_p^{-1}) to the period when $\Delta h_a = \Delta h_{a\ max}$, that is, until the period when the growth with this doping technology tends to the maximum value, there is an exponentially diminishing dependence (Figures 16(b) and (d)).

As the discharge energy rises, the thickness of the strengthened layer during alitisation increases and reaches its maximum value (Δh_{amax}). In addition, the increase h_a of the strengthened layer grows stronger, the

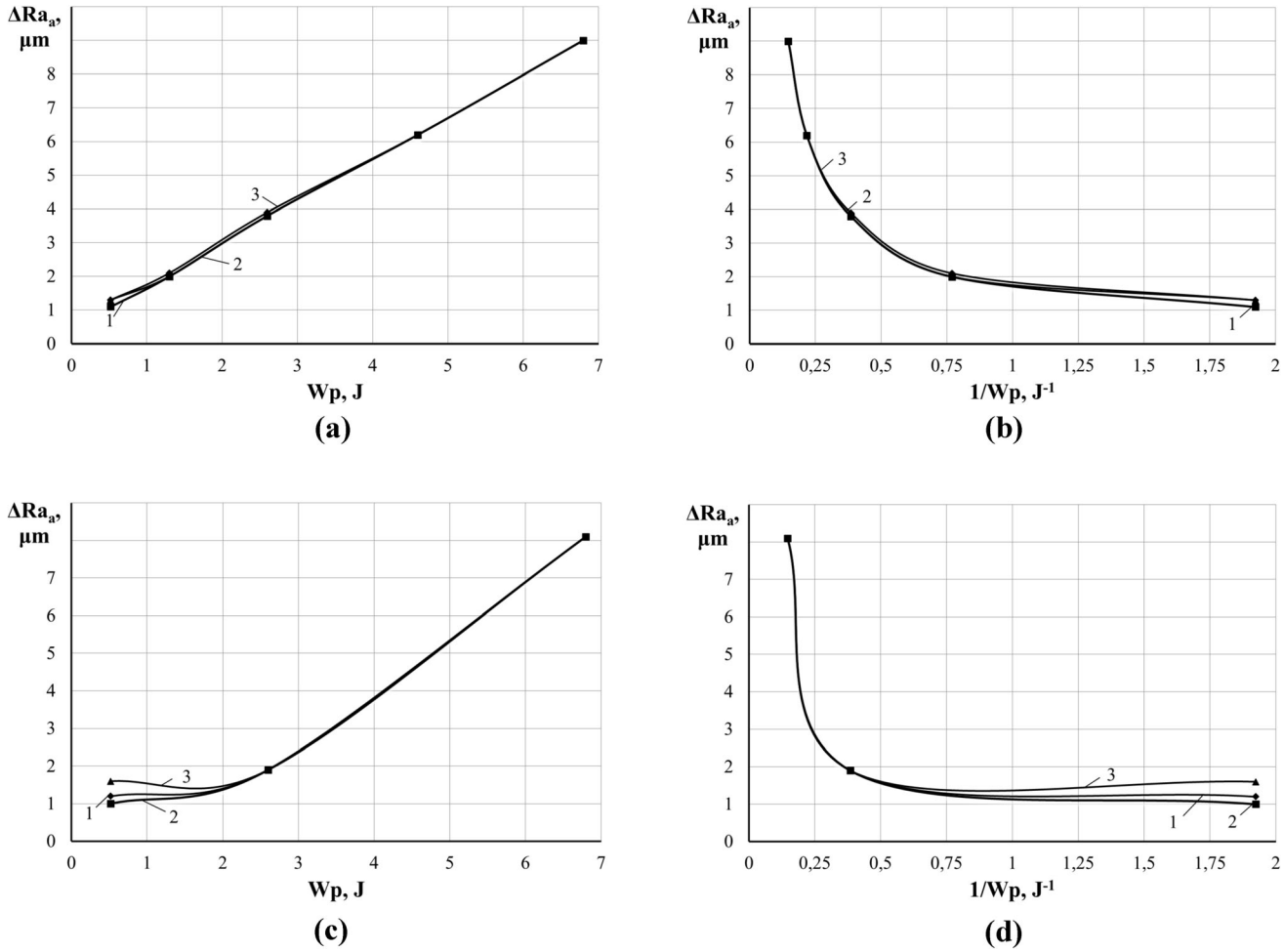

Fig. 18—Surface roughness as a function of ESA alitisation for steel C20 (*a*, *b*) and steel C40 (*c*, *d*): a, c—on the discharge energy W_p; b, d—on the value of the reverse discharge energy $1/W_p$. In graphs: 1: traditional ESA aluminisation technology; 2: productivity was reduced by about 2 factors (the 1st option, Table II); 3: productivity was reduced by about 4 factors (the 2nd option, Table II).

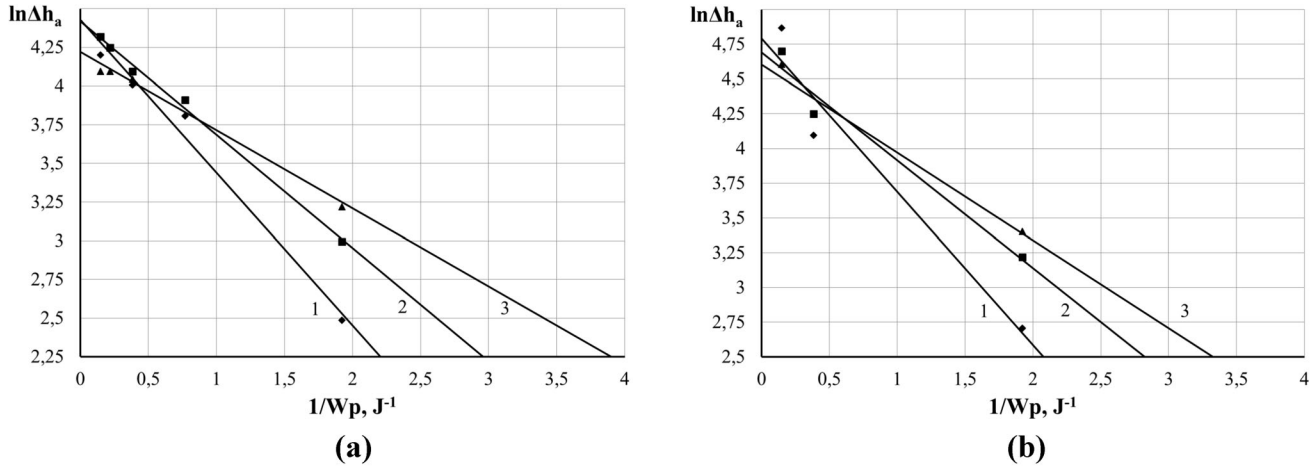

Fig. 19—Dependence of $\ln\Delta h_a$ on W_p^{-1} for the alitisation by the ESA method of the steels C20 (*a*) and C40 (*b*). In graphs: 1: traditional ESA aluminisation technology; 2: productivity was reduced by about 2 factors (the 1st option, Table II); 3: productivity was reduced by about 4 factors (the 2nd option, Table II).

greater the activation energy of the process of formation of the strengthened layer during ESA ($E_{a\Delta h}$).

From the experimental dependence of h_a on (W_p^{-1}) (approaching a decreasing exponent curve), it can be concluded that $\ln\Delta h_a$ is proportional to ($-\ W_p{}^{-1}$) and the value of $E_{a\Delta h}$, *i.e.*,

$$\ln \Delta h_a : \left(-W_p^{-1}\right),\ E_{a\Delta h}. \quad [1]$$

Moving from the approximate equation to the exact equation, the following is obtained:

$$\Delta h_a = \Delta h_{a\,max} \times e^{\frac{-E_{a\Delta h}}{W_p}}. \quad [2]$$

Equation [2] is called the equation for predicting the thickness of the hardened layer when alitising by the ESA method.

Using (2)

$$E_{a\Delta h} = W_p, \quad [3]$$

have:

$$\frac{\Delta h_a}{\Delta h_{a\,max}} = e^{-1}. \quad [4]$$

Therefore, $E_{a\Delta h}$ is a critical value equal to the discharge energy at which Δh_a is e times smaller than Δh_{amax}. Call it the constant of Eq. [2] for the prediction of the thickness of the hardened layer in the case of alitisation by the ESA method. The dimension $[E_{a\Delta h}] = J$.

Use a similar approach to analyse the dependence of the microhardness of the hardened layer when alitization by the ESA method $H_{\mu a}$ (Figure 17).

The equation for predicting the microhardness of the hardened layer during alitization by the ESA method

$$\Delta H_{\mu a} = \Delta H_{\mu a\ max} \times e^{\frac{-E_{a\Delta H_\mu}}{W_p}}. \quad [5]$$

In addition to the thickness and microhardness of the hardened layer, the roughness of the formed surface layer and its continuity are also affected by the ESA modes (discharge energy and productivity).

At the same time, the surface roughness changes significantly with the discharge energy when each individual energy pulse affects different volumes of the surface layer of both the anode (alloying electrode) and the cathode (part). As a result, at different values of discharge energy, a series of differently sized, more or less regularly spaced elevations and depressions with relatively small steps along the base length are formed on the surface of the part. If the productivity of the ESA, *i.e.*, the treatment time per unit area, is varied and the discharge energy is not varied, the effect of the unit energy pulses remains unchanged, *i.e.*, the size of the roughness peaks and valleys remains unchanged. This is confirmed by Figure 18, where all the roughness measurement results for different process powers fit on one line.

The proposed approach will be applied to the analysis of surface layer roughness dependencies Ra_a when alitization by the ESA method. The equation for predicting surface roughness at alitization by the ESA method:

$$\Delta Ra_a = \Delta Ra_{a\,max} \times e^{\frac{-E_{a\Delta Ra}}{W_p}}. \quad [6]$$

The equation for predicting layer continuity at alitization by the ESA method:

$$\Delta S_a = \Delta S_{a\,max} \times e^{\frac{-E_{a\Delta S}}{W_p}}. \quad [7]$$

Equations [2], [5] through [7] can be used to determine the ESA mode required to obtain the desired thickness and microhardness of the hardened layer, roughness and continuity of the surface layer during ESA alitisation. Then:

$$N_p = \frac{E_{a\Delta Ra}}{\ln\frac{\Delta Ra_{a\,max}}{\Delta Ra_x}};\quad N_p = \frac{E_{a\Delta S}}{\ln\frac{\Delta S_{a\,max}}{\Delta S_x}}. \quad [8]$$

According to Eq. [2], there should be a linear relationship between the logarithm of the thickness of the cured layer and the value of the reverse discharge energy. Plotting dependency graphs $\ln\Delta h_a$ from (W_p^{-1}).

The dependence of $\ln\Delta h_a$ on $W_p{}^{-1}$ for the aluminisation of steel C20 by the ESA method tends to be a straight line, as can be seen from Figure 19. The values of the tangents of the angles of inclination of the lines to the abscissa in the region of exponentially decreasing dependence are given in Table VII.

The pre-exponential factor (Table VII) is found by the segment truncated on the axis of the ordinates of the direct exponentially decreasing dependence $\ln\Delta h_a$ from $W_p{}^{-1}$ (Figure 19), extended to the value of the abscissa $W_p{}^{-1} = 0$ ($\ln\Delta h_a = \ln\Delta h_{amax}$ at $W_p{}^{-1} \to 0$).

Activation energy calculation results $E_{a\Delta h}$ (constants of Eq. [2]) for predicting the thickness of the strengthened layer during alitisation using the ESA method, determined in two ways, the first, when $E_{a\Delta h} = W_p$, the second—at $E_{a\Delta h} = |tg\alpha|$, are given in Table VII.

Some incompatibility of the values of ESA constants $E_{a\Delta h}$ (up to 7 pct), determined by different methods, can be explained as a consequence of various measurement errors. In general, the convergence of the results is satisfactory.

The proposed approach to calculations can be used to determine

- activation energy constants ($E_{a\Delta H_\mu}$) and the constants of the equation for predicting the microhardness of the hardened layer during alitization by the ESA method of the steels;
- activation energy constants ($E_{a\Delta Ra}$) and constants of the equation for predicting surface roughness during alitization by the ESA;
- activation energy constants ($E_{q\Delta S}$) and the constants of the equation for predicting the integrity of the

Table VII. Calculation of the Activation Energy Constant ($E_{a\Delta h}$) and the Constants of the Equation for Predicting the Thickness of the Strengthened Layer During Alitization by the ESA Method of Steels C20 (in the Numerator) and C40 (in the Denominator) at Different Productivity

ESA Mode	$E_{a\Delta h} = \lvert tg\alpha \rvert$ (J)	$E_{a\Delta h} = W_p$ (J)	Pct	$\Delta h_{a\,max}$(μm)
Traditional ESA Technology	0.989 1.10	0.99 1.17	1 6	74 120
Productivity Was Reduced by About 2 Factors (the 1st Option, Table II)	0.732 0.775	0.74 0.83	1 7	82 108
Productivity Was Reduced by About 4 Factors (the 2nd Option, Table II)	0.505 0.632	0.49 0.68	3 7	68 99

Table VIII. Summary of ESA Constants for Alitisation of C20 (Numerator) and C40 (Denominator) Steels at Different Productivities

ESA Mode	$E_{a\Delta h} = \lvert tg\alpha \rvert$ (J)	Δh_{amax} (μm)	$E_{a\Delta H_\mu} = \lvert tg\alpha \rvert$(J)	$\Delta h_{a\mu max}$ (MPa)	$E_{a\Delta Ra} = \lvert tg\alpha \rvert$ (J)	ΔRa_{amax} (μm)	$E_{a\Delta S} = \lvert tg\alpha \rvert$ (J)	ΔS_{amax} (Pct)
Traditional ESA Technology	0.989 1.10	74 120	0.588 1.10	5472 7498	0.96 0.904	7 5	0.29 0.364	100
Productivity Was Reduced by About 2 Factors (the 1st Option, Table II)	0.732 0.775	82 108	0.557 0.775	5606 7544	1056 0.797	7.17 5.2	0.125 0.279	100
Productivity Was Reduced by About 4 Factors (the 2nd Option, Table II)	0.505 0.632	68 99	0.542 0.63	5579 7625	0.95 0.625	7.18 4.2	0.272 0.03	100

layer during alitization by the ESA method for different productivities.

The summarized data of ESA constants, necessary for calculating the quality parameters of the surface layer, are given in Table VIII.

The analysis of Table VIII shows that as the productivity decreases, i.e. as the treatment time per unit area of a part (labour intensity of the ESA process) increases, the values of the ESA constants for the aluminised steels C20 and C40 decrease. This can be explained by the fact that with each successive cycle the amount of material transferred from the anode to the cathode decreases, *i.e.*, the aluminisation process 'slows down', saturation occurs, which is typical of exponential dependencies. At the same time, the effect of the aluminisation process on the quality parameters of the surface layers of the parts (thickness of the "white" layer and the diffusion zone, microhardness, continuity, roughness) also decreases.

It is important to state that the proposed mathematical model serves as an effective predictive tool for optimizing ESA parameters to achieve aluminized coatings with tailored characteristics such as thickness, microhardness, surface roughness, and continuity. Based on a combination of theoretical insights and experimental validation, the model relates coating quality indicators to ESA parameters, specifically discharge energy (W_p) and treatment time (reverse productivity). Importantly, the model allows rapid prediction without the need to repeat full-scale experiments for each new treatment condition. The model also accommodates both traditional and reduced productivity, allowing flexible adaptation to manufacturing conditions. By determining important parameters such as maximum thickness, hardness and roughness during ESA processing in certain modes, the model helps to avoid overtreatment, which can compromise the continuity of the coating and thus its quality. Overall, the model algorithm provides a reliable basis for process planning and control of ESA, reducing the number of experiments, increasing treatment efficiency and improving coating quality.

To address the issue of validation, a comparative analysis was carried out using data from published studies—for alitisation[41] and nitrocementation[63] by ESA. The changes in the coating characteristics as a function of the energy parameters of the treatment predicted by the developed model, in particular the exponential dependence of the hardened layer thickness and microhardness on the inverse of the discharge energy, are in agreement with the experimental data reported in these papers. For example, the layer thickness values obtained for certain ESA parameters are within ± 10 pct of the values reported in Reference 41 for the alitisation of a steel substrate at classical ESA productivity (Table I). In addition, the trends in roughness and continuity change predicted by the equations also agree with the experimental results, confirming the reliability of the model for different electrode material systems.

Although the model parameters were derived from an experimental data set, the consistency of the results with external studies supports the generalisability of the model. Given the multi-parameter nature of the electrospark alloying process, the authors recognise the importance of further refinement of the mathematical model. Future development should aim to incorporate a wider range of influencing variables—such as electrode material properties, pulse frequency, interelectrode gap

and environmental conditions—to improve the accuracy of predictions regarding the structure and properties of ESA coatings. This will enhance the ability of the model to serve as a comprehensive tool for process optimisation in various technological contexts.

V. CONCLUSIONS

(1) An analysis of the literature to identify trends in improving the wear and heat resistance of materials has shown that an effective and economical way to increase the durability of parts is to create functional coatings on working surfaces. The electrospark alloying (ESA) is energy efficient, environmentally friendly and has a number of other advantages. It allows the creation of surface structures with unique physical and mechanical properties.

(2) The peculiarities of microstructure formation during the alloying of steels C20 and C40 under different modes and methods of ESA are considered. The ''traditional'' alloying modes, ESA with an aluminium electrode and modes with reduced productivity (by a factor of 2 and 4) were studied.

(3) With the classic ESA process productivity values, the layer structure consists of three areas: 'white' layer, diffusion zone and substrate metal. As the discharge energy rises, the qualitative parameters of the surface layer increase, such as thickness, microhardness of the 'white' layer and the transition zone, and roughness. Increasing the discharge energy during ESA leads to a change in the chemical and phase composition of the layer: at low discharge energies, a layer is formed that consists mainly of α-Fe and aluminium oxides; as the discharge energy rises, the layer consists of iron and aluminium intermetallics as well as free aluminium.

(4) An analysis of the structure and properties of the surface layers of steel parts after alitisation by the ESA method with reduced productivity was carried out. Two options of productivity reduction were studied in relation to the traditional one: the first one with productivity reduced by a factor of 2; the second one with productivity reduced by a factor of 4. With a 2-fold decrease in productivity and an increase in discharge energy, the thickness of the 'white' layer increases to 75 to 110 μm; the microhardness of the 'white' layer rises to 7450 MPa; the coating continuity tends to 100 pct. With a 4-fold decrease in productivity and an increase in discharge energy, the thickness of the 'white' layer also increases, but not intensively, to 60 μm at W_p = 4.6 J and then does not change; the microhardness of the 'white' layer rises to 7300 MPa; at the same time, the surface roughness Ra rises to 8.1 to 9.0 μm and the continuity is 95 pct. A 4-fold decrease in productivity contributes to a deterioration in the quality parameters of the coating and an increase in roughness.

(5) The equations of the mathematical model and methods for determining the constants of the equations for predicting the thickness of the aluminised layer, the maximum microhardness of the surface layer, the maximum surface roughness and the maximum layer continuity when aluminising C20 and C40 steels by the ESA method are proposed. An algorithm has been developed and the adequacy of the mathematical model has been verified, which makes it possible to predict the main technological parameters of ESA in order to obtain a coating with the specified quality indicators.

FUNDING

Some of the results have been obtained within the research projects ''Development of environmentally safe technologies for surface modification of power plant equipment parts using combined methods based on electrospark alloying'' (State Reg. No. 0124U000539), Sumy State University, funded by the Ministry of Education and Science of Ukraine.

CONFLICT OF INTEREST

On behalf of all authors, the corresponding author states that there is no conflict of interest.

REFERENCES

1. M. Juhl, M.Z. Hauschild, and K. Dam-Johansen: *Prog. Org. Coat.*, 2024, vol. 197, 108781https://doi.org/10.1016/j.porgcoat.2024.108781.
2. R. Nartita, D. Ionita, and I. Demetrescu: *Sustainability*, 2021, vol. 13, p. 10217. https://doi.org/10.3390/su131810217.

3. J. Krmela, T. Hovorun, K. Berladir, and A. Artyukhov: *Manuf. Technol.*, 2021, vol. 21(2), pp. 206–12. https://doi.org/10.21062/mft.2021.034.
4. Y. Ju, I. Konoplianchenko, J. Pu, Z. Zhang, Q. Dong, and M. Dumanchuk: *Results Eng.*, 2024, vol. 21, p. 101985. https://doi.org/10.1016/j.rineng.2024.101985.
5. D.B. Hlushkova, V.M. Volchuk, P.M. Polyansky, V.A. Saenko, and A.A. Efimenko: *Funct. Mater.*, 2023, vol. 30(2), pp. 275–81. https://doi.org/10.15407/fm30.02.275.
6. Y. Liu, S. Zhang, W. Shao, Z. Wang, J. Qu, W. Zhou, and S. Zhang: *Coatings*, 2025, vol. 15, p. 88. https://doi.org/10.3390/coatings15010088.
7. Y.X. Ou, H.Q. Wang, X. Ouyang, Y.Y. Zhao, Q. Zhou, C.W. Luo, Q.S. Hua, X.P. Ouyang, and S. Zhang: *Prog. Mater. Sci.*, 2023, vol. 136, 101125https://doi.org/10.1016/j.pmatsci.2023.101125.
8. B. Fotovvati, N. Namdari, and A. Dehghanghadikolaei: *J. Manuf. Mater. Process.*, 2019, vol. 3, p. 28. https://doi.org/10.3390/jmmp3010028.
9. O.P. Gaponova, B. Antoszewski, V.B. Tarelnyk, P. Kurp, O.M. Myslyvchenko, and N.V. Tarelnyk: *Materials*, 2021, vol. 14, p. 6332. https://doi.org/10.3390/ma14216332.
10. V.B. Tarel'nik, V.S. Martsinkovskii, and A.N. Zhukov: *Chem. Pet. Eng.*, 2017, vol. 53, pp. 385–89. https://doi.org/10.1007/s10556-017-0351-5.
11. O. Umanskyi, M. Storozhenko, V. Tarelnyk, O. Koval, Yu. Gubin, N. Tarelnyk, and T.V. Kurinna: *Powder Metall. Met. Ceram.*, 2020, vol. 59, pp. 57–67. https://doi.org/10.1007/s11106-020-00138-5.
12. V.B. Tarelnyk, O.P. Gaponova, V.B. Loboda, E.V. Konoplyanchenko, V.S. Martsinkovskii, Y.I. Semirnenko, N.V. Tarelnyk, M.A. Mikulina, and B.A. Sarzhanov: *Surf. Eng. Appl. Electrochem.*, 2021, vol. 57, pp. 173–84. https://doi.org/10.3103/S1068375521020113.
13. E.A. Esfahani, H. Salimijazi, M.A. Golozar, J. Mostaghimi, and L. Pershin: *J. Therm. Spray Technol.*, 2012, vol. 21, pp. 1195–202. https://doi.org/10.1007/s11666-012-9810-x.
14. T. Chmielewski, P. Siwek, M. Chmielewski, A. Piątkowska, A. Grabias, and D. Golański: *Metals*, 2018, vol. 8, p. 1059. https://doi.org/10.3390/met8121059.
15. N.V. Bangaru and R.C. Krutenat: *J. Vac. Sci. Technol.*, 1984, vol. 2, pp. 806–15. https://doi.org/10.1116/1.582882.
16. K. Kostyk, M. Hatala, V. Kostyk, V. Ivanov, I. Pavlenko, and D. Duplakova: *Processes*, 2021, vol. 9, p. 698. https://doi.org/10.3390/pr9040698.
17. A.D. Pogrebnjak, V.I. Ivashchenko, P.L. Skrynskyy, O.V. Bondar, P. Konarski, K. Zaleski, S. Jurga, and E. Coy: *Composites B*, 2018, vol. 142, pp. 85–94. https://doi.org/10.1016/j.compositesb.2018.01.004.
18. O.D. Pogrebnjak, K.O. Dyadyura, and O.P. Gaponova: *Metallofiz. Noveishie Tekhnol.*, 2015, vol. 37(7), pp. 899–919. https://doi.org/10.15407/mfint.37.07.0899.
19. B. Antoszewski, S. Tofil, M. Scendo, and V. Tarelnik: *IOP Conf. Ser. Mater. Sci. Eng.*, 2017, vol. 233, 012036https://doi.org/10.1088/1757-899X/233/1/012036.
20. J. Górka, A. Lont, D. Janicki, T. Poloczek, and A. Rzeźnikiewicz: *Coatings*, 2024, vol. 14, p. 646. https://doi.org/10.3390/coatings14050646.
21. B. Antoszewski, O.P. Gaponova, V.B. Tarelnyk, O.M. Myslyvchenko, P. Kurp, T.I. Zhylenko, and I. Konoplianchenko: *Materials*, 2021, vol. 14, p. 739. https://doi.org/10.3390/ma14040739.
22. J. Wang, M. Zhang, S. Dai, and L. Zhu: *Coatings*, 2023, vol. 13, p. 1473. https://doi.org/10.3390/coatings13081473.
23. O.M. Myslyvchenko, O.P. Gaponova, V.B. Tarelnyk, and M.O. Krapivka: *Powder Metall. Met. Ceram.*, 2020, vol. 59, pp. 201–08. https://doi.org/10.1007/s11106-020-00152-7.
24. V.B. Tarel'nik, V.S. Martsinkovskii, E.V. Konoplyanchenko, A.V. Belous, and O.P. Gaponova: *Chem. Pet. Eng.*, 2018, vol. 54, pp. 598–604. https://doi.org/10.1007/s10556-018-0521-0.
25. V. Tarelnyk, I. Konoplianchenko, V. Martsynkovskyy, A. Zhukov, and P. Kurp: *Advances in Design, Simulation and Manufacturing. DSMIE 2019. Lecture Notes in Mechanical Engineering*, 2019. https://doi.org/10.1007/978-3-319-93587-4_40.
26. V.B. Tarelnyk, I.V. Konoplianchenko, O.P. Gaponova, N.V. Tarelnyk, V.S. Martsynkovskyy, B.O. Sarzhanov, O.A. Sarzhanov, and B. Antoszewski: *Powder Metall. Met. Ceram.*, 2020, vol. 58, pp. 703–13. https://doi.org/10.1007/s11106-020-00127-8.
27. V.B. Tarel'nik, A.V. Paustovskii, Yu.G. Tkachenko, V.S. Martsinkovskii, E.V. Konoplyanchenko, and K. Antoshevskii: *Surf. Eng. Appl. Electrochem.*, 2017, vol. 53, pp. 285–94. https://doi.org/10.3103/S1068375517030140.
28. L.P. Kornienko, G.P. Chernova, V.V. Mihailov, and A.E. Gitlevich: *Surf. Eng. Appl. Electrochem.*, 2011, vol. 47, pp. 9–17. https://doi.org/10.3103/S106837551101011X.
29. V. Martsynkovskyy, V. Tarelnyk, I. Konoplianchenko, O. Gaponova, and M. Dumanchuk: *Advances in Design, Simulation and Manufacturing II. DSMIE 2019. Lecture Notes in Mechanical Engineering*, 2020. https://doi.org/10.1007/978-3-030-22365-6_22.
30. M. Rukanskis: *Surf. Eng. Appl. Electrochem.*, 2019, vol. 55, pp. 607–19. https://doi.org/10.3103/S1068375519050107.
31. V.B. Tarelnyk, O.P. Gaponova, Y.V. Konoplianchenko, V.S. Martsynkovskyy, N.V. Tarelnyk, and O.O. Vasylenko: *Metallofiz. Noveishie Tekhnol.*, 2019, vol. 41, pp. 173–92. https://doi.org/10.15407/mfint.41.02.0173.
32. V.B. Tarelnyk, O.P. Gaponova, Y.V. Konoplianchenko, V.S. Martsynkovskyy, N.V. Tarelnyk, and O.O. Vasylenko: *Metallofiz. Noveishie Tekhnol.*, 2019, vol. 41, pp. 313–35. https://doi.org/10.15407/mfint.41.03.0313.
33. V.B. Tarel'nik, E.V. Konoplyanchenko, P.V. Kosenko, and V.S. Martsinkovskii: *Chem. Pet. Eng.*, 2017, vol. 53, pp. 540–46. https://doi.org/10.1007/s10556-017-0378-7.
34. P. Leo, G. Renna, and G. Casalino: *Appl. Sci.*, 2017, vol. 7, p. 945.
35. W.J. Cheng and C.J. Wang: *Appl. Surf. Sci.*, 2011, vol. 257(10), pp. 4663–668. https://doi.org/10.1016/j.apsusc.2010.12.118.
36. M. Brochu, J.G. Portillo, J. Milligan, and D.W. Heard: *Open Surf. Sci. J.*, 2011, vol. 105(3), pp. 105–14. https://doi.org/10.2174/1876531901103010105.
37. P. Huilgol, K. Rajendra Udupa, and K. Udaya Bhat: *Surf. Coat. Technol.*, 2019, vol. 375, pp. 544–53. https://doi.org/10.1016/j.surfcoat.2019.07.031.
38. P. Huilgol, K. Udaya Bhat, and K. Rajendra Udupa: *Mater. Today Proc.*, 2018, vol. 5(11), pp. 24702–4709. https://doi.org/10.1016/j.matpr.2018.10.268.
39. P. Huilgol, K. Rajendra Udupa, and K. Udaya Bhat: *Surf. Coat. Technol.*, 2018, vol. 348, pp. 22–30. https://doi.org/10.1016/j.surfcoat.2018.05.013.
40. J.H. Westbrook, and R.L. Fleischer: *Intermetallic Compounds—Principles and Practice: Progress*, Wiley, 2002. https://doi.org/10.1002/0470845856.
41. G.V. Kirik, O.P. Gaponova, V.B. Tarelnyk, O.M. Myslyvchenko, and B. Antoszewski: *Powder Metall. Met. Ceram.*, 2018, vol. 56, pp. 688–96. https://doi.org/10.1007/s11106-018-9944-6.
42. V.B. Tarelnyk, O.P. Gaponova, and O.M. Myslyvchenko: *Metallofiz. Noveishie Tekhnol.*, 2019, vol. 41, pp. 1377–394. https://doi.org/10.15407/mfint.41.10.1377.
43. V.B. Tarelnyk: *Quality Control of Surface Layers of Parts by Combined Electroerosive Alloying*, Publishing House 'MacDen, Sumy, 2002. (**in Russian**).
44. S.V. Nikolenko, A.D. Verkhoturov, N.A. Syui, and E.N. Kuz'michev: *Surf. Eng. Appl. Electrochem.*, 2016, vol. 52, pp. 342–49. https://doi.org/10.3103/S1068375516040098.
45. C. Barile, C. Casavola, G. Pappalettera, and G. Renna: *Coatings*, 2022, vol. 12, p. 1536. https://doi.org/10.3390/coatings12101536.
46. P. Matysik, S. Jóźwiak, and T. Czujko: *Materials*, 2015, vol. 8, pp. 914–31. https://doi.org/10.3390/ma8030914.
47. X. Hong, Y. Tan, C. Zhou, T. Xu, and Zh. Zhang: *Appl. Surf. Sci.*, 2015, vol. 356, pp. 1244–251. https://doi.org/10.1016/j.apsusc.2015.08.233.
48. N. Radek, J. Bronček, P. Fabian, J. Pietraszek, and K. Antoszewski: *Mater. Sci. Forum*, 2015, vol. 818, pp. 61–4. https://doi.org/10.4028/www.scientific.net/msf.818.61.
49. Z. Jiao, S. Peterkin, L. Felix, R. Liang, J.P. Oliveira, N. Schell, N. Scotchmer, E. Toyserkani, and Y. Zhou: *J. Mater. Eng. Perform.*, 2018, vol. 27, pp. 4799–809. https://doi.org/10.1007/s11665-018-3579-0.
50. G. Renna, P. Leo, G. Casalino, and E. Cerri: *Adv. Mater. Sci. Eng.*, 2018, https://doi.org/10.1155/2018/8563054.

51. Y. Wei, A. Feng, C. Chen, D. Shang, X. Pan, and J. Xue: *Coatings*, 2023, vol. 13, p. 1039. https://doi.org/10.3390/coatings13061039.
52. A. Lešnjak and J. Tušek: *Sci. Technol. Weld. Join.*, 2002, vol. 7(6), pp. 391–96. https://doi.org/10.1179/136217102225006886.
53. T. Penyashki, G. Kostadinov, M. Kandeva, A. Nikolov, R. Dimitrova, V. Kamburov, P. Danailov, and S. Bozhkov: *Tribol. Ind.*, 2023, vol. 46(1), pp. 13–28. https://doi.org/10.24874/ti.1508.06.23.08.
54. O. Sahin and A.V. Ribalko: *Mass Transfer-Advanced Aspects*, InTech, London, 2011. https://doi.org/10.5772/24339.
55. K. Korkmaz, A.V. Ribalko, and O. Sahin: *Met. Mater.*, 2013, vol. 51, pp. 283–89. https://doi.org/10.4149/km20135283.
56. D. Marchenko and K. Matvyeyeva: *Probl. Tribol.*, 2023, vol. 28, pp. 65–72.
57. N. Radek, J. Pietraszek, and A. Szczotok: *Proceedings 26th International Conference on Metallurgy and Materials*, 2017, pp. 1432–37.
58. M.S. Storozhenko, O.P. Umanskyi, V.B. Tarelnyk, OYu. Koval, Yu.V. Gubin, M.O. Mikulina, I.S. Martsenyuk, O.D. Kostenko, and T.V. Kurinna: *Powder Metall. Met. Ceram.*, 2020, vol. 59, pp. 330–41.
59. V. Tarelnyk, O. Gaponova, O. Myslyvchenko, and B.O. Sarzhanov: *Powder Metall. Met. Ceram.*, 2020, vol. 59, pp. 76–88. https://doi.org/10.1007/s11106-020-00152-7.
60. C. Barile, C. Casavola, G. Pappalettera, and G. Renna: *Coatings*, 2022, vol. 12, p. 1536.
61. R.J. Borg and G.J. Dienes: *An Introduction to Solid State Diffusion*, Academic, San Diego, 2012.
62. O.Y. Dubei, T.F. Tutko, L.Y. Ropyak, and M.V. Shovkoplias: *Metallofiz. Noveishie Tekhnol.*, 2022, vol. 44(2), pp. 251–72. https://doi.org/10.15407/mfint.44.02.0251.
63. O.P. Gaponova, V.B. Tarelnyk, B. Antoszewski, N. Radek, N.V. Tarelnyk, P. Kurp, O.M. Myslyvchenko, and J. Hoffman: *Materials*, 2022, vol. 15, p. 6085. https://doi.org/10.3390/ma15176085.